Synthesis of Vanadium Oxide (V_2O_5) Nanoparticles for Degradation of Methylene Blue Dye

Demise Sorie Tufa

A Thesis Submitted to the Department of Applied Chemistry, College of Applied Natural Sciences

In Partial Fulfillment of the Requirements for the Degree of Master of Science in Applied Chemistry (Industrial Chemistry)

Office of Graduate Studies
Adama Science and Technology University

June, 2025

Adama, Ethiopia

Synthesis of Vanadium Oxide (V_2O_5) Nanoparticles for Degradation of Methylene Blue Dye

Demise Sorie Tufa

Advisor: Dr. Fedlu Kedir (Associate Professor)

A Thesis Submitted to the Department of Applied Chemistry, College of Applied Natural Sciences

In Partial Fulfillment of the Requirements for the Degree of Master of Science in Applied Chemistry (Industrial Chemistry)

Office of Graduate Studies

Adama Science and Technology University

June, 2025

Adama, Ethiopia

DECLARATION

I hereby declare that this master's thesis entitled "Synthesis of Vanadium Oxide (V_2O_5) Nanoparticles for Degradation of Methylene Blue Dye" is my own work and has not been submitted to any university for a similar purpose. The reference used in this thesis is duly recognized by proper citation.

Demise Sorie Tufa _____ _____

Signature Date

RECOMMENDATION

I, the advisor of this thesis, hereby certify that I have advised the student while developing this thesis and read the draft of the thesis entitled "Synthesis of Vanadium Oxide (V_2O_5) Nanoparticles for Degradation of Methylene Blue Dye" prepared under my guidance by Demise Sorie Tufa. Therefore, I recommend the submission of the thesis to the department for future review and evaluation.

Dr. Fedlu Kedir (Associate Professor) _____ _____

Advisor Signature Date

APPROVAL PAGE

I hereby certify that the recommendations and suggestions given by the thesis review committee have been appropriately incorporated into the final thesis entitled "Synthesis of Vanadium Oxide (V_2O_5) Nanoparticles for Degradation of Methylene Blue Dye" by Demise Sorie Tufa.

Dr. Fedlu Kedir (Associate Professor) _____ _____

Advisor Signature Date

We, the undersigned, members of the Board of Examiners of the thesis paper open defense by Demise Sorie Tufa, have read and evaluated the thesis entitled "Synthesis of Vanadium Oxide (V_2O_5) Nanoparticles for Degradation of Methylene Blue Dye" and assessed the understanding of the candidate about the proposed research. This is, therefore, to certify that the thesis is accepted, and we recommend the implementation of the thesis.

_____ _____ _____

Chairperson Signature Date

_____ _____ _____

Internal Examiner Signature Date

Ararso Nagari Wagassa, PhD 03/10/2025

External Examiner Signature Date

Finally, approval and acceptance of the thesis are contingent upon submission of its final copy to the Office of Postgraduate Studies (OPGS) through the Department Graduate Council (DGC) and School Graduate Committee (SGC).

_____ _____ _____

Department Head Signature Date

_____ _____ _____

School Dean Signature Date

_____ _____ _____

Office of Postgraduate studies, Dean Signature Date

ACKNOWLEDGMENT

I am grateful to the Almighty God for the good health and well-being necessary to complete this work. To Him alone, I give all glory. I would like to give my honorable thanks to Adama Science and Technology University as a whole and the Department of Applied Chemistry in particular for giving me this opportunity. First and foremost, the completion of this thesis would not have been possible without the excellent guidance, support, respect, and friendship of my advisor, Dr. Fedlu Kedir (Associate Professor).

His positive influence will always be a guide as I venture out on my own to tackle challenging scientific problems. I am lucky to be guided and advised by him, and in general his brotherly and humble approach makes me successful. I acknowledge all his encouragement and the valuable time he has given me with deep gratitude and appreciation.

I would like to extend my heartfelt gratitude to Mr. Guta for the help with assistance in analyses during my experimental work. I have been indebted to my colleagues Mr. Hatamu Tedese, Mr. Eshetu Megersa, and Mr. Tilahun Zeleke for their invaluable advice, constructive comments, and fruitful discussion.

I would like to express my sincere gratitude to the Awash Melkassa Chemical Factory for providing all the necessary assistance and facilities to conduct my thesis work. I also express my genuine heartfelt gratitude to all workers of the factory, especially the Quality Control Laboratory staff members, for their help with my work. I never forgot your great contribution.

TABLE OF CONTENTS

LIST OF TABLES

LIST OF FIGURES

LIST OF ABBREVIATIONS AND ACRONYMS

AOPs	Advanced oxidation processes
AOT	Sulphosuccinic acid bis (2-ethylhexyl) ester sodium salt
CE	Counter electrode
CTAB	Cetyl Trimethy Ammonium Bromide
SDS	Sodium Dodecyl Sulphate
CVD	Chemical vapor deposition
DSSC	Dye-sensitized solar cells
FESEM	Field emission Scanning electron microscopy
HUMO	Highest occupied molecular orbital
LUMO	Lowest unoccupied molecular orbital
PECDV	Plasma-enhanced Chemical vapor deposition
PICVD	Photo-initiated Chemical vapor deposition
SCR	Selective catalytic reduction
TACVD	Thermally activated Chemical vapor deposition
UV-Vis	UV–Vis diffuse reflectance spectrophotometer
$VOSO_4$	Oxovanadium sulfate (Vanadyl Sulfate)
XRD	Energy Dispersive X-ray Diffraction

ABSTRACT

Vanadium pentoxide (V_2O_5) nanoparticles were successfully synthesized using ammonium metavanadate as a precursor and Laggera tomentosa leaf extract as a natural reducing agent through a sol–gel method. The obtained nanoparticles were characterized to investigate their morphology, optical properties, functional groups, and structural features using ultraviolet–visible diffuse reflectance spectroscopy (UV–vis DRS), Fourier transform infrared spectroscopy (FT–IR), Brunauer–Emmett–Teller (BET) surface area analysis, X-ray diffraction (XRD), and scanning electron microscopy (SEM). The photocatalytic performance of the V_2O_5 nanocomposite was evaluated under visible light irradiation for the degradation of methylene blue (MB), with optimization of both catalyst dosage and contact time.

***Keywords**: Vanadium pentoxide, green synthesis method, methylene blue, photocatalysis, dye degradation.*

1 INTRODUCTION

1.1 Background of the study

In recent years, nanotechnology has gained more attention. Nanoscale technology includes materials with a size between 1 and 100 nanometers. (Singh, 2022). The term "nanotechnology" describes the process of creating, representing, modifying, and utilizing structures by managing their size and form at the nanoscale (Bayda et al., 2020). Synthesis of nanoparticles is gaining widespread popularity worldwide (Rafique et al., 2016), and nanotechnology is the most dynamic field of material sciences studies. The progress and development of nanotechnology have resulted in a revolution in living on the planet by virtue of its use in multiple domains. It has also introduced a new thinking and a broader awareness of what man can do through controlling significance at the nanoscale. Nanoparticles (NPs), unlike their bulk counterparts, are better contenders for application performances in that they possess the unique characteristic of possessing a huge surface-to-volume ratio (Kushwaha et al., 2021).

The intrinsic properties of the NPs are employed in various applications such as photocatalysis, electronics, medical devices, cosmetics, packaging, environmental cleaning, energy storage, agriculture, vehicles, and information technology. Among all the massive applications of current nanoparticles, metal oxide nanoparticles (MONPs) proved to be more acceptable as they have exceptional physical, chemical, and biological properties. The employment of poisonous chemicals as capping agents and for reduction during nanoparticle synthesis produces a series of adverse effects and toxicity (Demissie et al., 2020). The recent discovery of nanoparticles has produced encroachments in the subject of nanotechnology with the help of the formation of a series of successful methods for synthesizing NPs with the desired shapes and sizes according to certain demands. The field of nanotechnology has experienced great expansion in the recent past, from a diverse range of research in material science, biomedical science, chemical science, and contemporary industry. NPs have a very high surface area to volume ratio compared to their bulk counterpart, which provides them with unique, remarkable, and enhanced physical and chemical properties. (Demissie et al., 2020).

The application of nanoparticles and nanomaterials has been rapidly expanding across numerous fields. They are now widely utilized in medicine, optics, cosmetics, biomedical devices, environmental remediation, the chemical industry, electronics, photocatalysis, energy storage, agriculture, the automotive sector, packaging, space technology, information technology,

sensors, catalysis, surface coatings, antimicrobial bandages, light-emitting devices, mechanical systems, textiles, and water purification (Demissie et al., 2020). Due to their tiny size, physical characteristics, and orientation, which seem to alter the behavior of any other material that comes into contact with them, nanoparticles are utilized widely. Exercising a multiplicity of physical, chemical, and biological approaches, these particles may be made with ease. The term "nanometallic materials" refers to metals and mixtures that create nanocrystalline granules with particle sizes between 5 and 100 nanometers. In comparison to their non-nano or bulk counterparts, nanoscale metals have a larger surface area (Kushwaha et al., 2021). Additionally, because of their small size, surface interaction, and quantum effects, they have distinct physical and chemical properties not found in non-nano metals. Nanoscale metals come in a variety of forms and have diverse uses in engineering, biology, and medicine (Ying et al., 2022).

Metal oxide nanoparticles have really caught the attention of materials chemists because of their wide range of potential applications. Specifically, one-dimensional (1D) nanostructured transition metal oxides are particularly prized for their distinctive magnetic, optical, and electrical characteristics, as well as their remarkable chemical and thermal stability. Because of these characteristics, they are valuable in a variety of industries, including sensing, energy storage, information technology, medicine, and catalysis. As a result, there is a lot of research being done to create effective synthetic pathways for their production (Corr, 2012). Vanadium oxide is an intriguing material that has acquired popularity in the realm of contemporary technical and commercial applications because of its simplicity of synthesis and inexpensive, high-specific-capacity components. Additionally, the substance has a high energy density, excellent safety-related qualities, and widespread resource availability at a fair cost. Due to its stability and favorable electrochemical qualities, the vanadium pentoxide form of oxides has attracted a lot of interest for more than ten years (T. R. Kishan Chand, H. M. Kalpana, 2022). Vanadium oxide is an interesting material that has gained more attention in the area of new technical and commercial processes owing to the simplicity of production and low-cost, high-specific-capacity material. Moreover, the material possesses high energy density, improved safety-related properties, and extensive resource availability at a low cost. Owing to stability and good electrochemical properties, the vanadium pentoxide phase of oxides has been highly in the spotlight for over a decade.

The world is experiencing a severe water pollution issue as a result of industrialization in recent years. Potable water is being contaminated by a variety of pollutants, including organic dyes, pesticides, and medicines, as a result of significant advancements in the industrial and agricultural industries. The amount of these dangerous and irreversible pollutants in the air and water is rising every day. The issue with these pollutants is that they endure in the earth for a long time and do not break down naturally. Rhodamine B (RhB), Congo red, and Methylene blue (MB) are just a few illustrations of the many dyes that are commonly discharged into drinkable water. One of the primary dyes created by the textile industry is MB, which is also known to be harmful to the environment and carcinogenic to people. In order to lessen water pollution and convert it into usable water, such dangerous pollutants must be broken down. Due to major advancements in research fields, various techniques have been created to break down dyes and transform polluted water into usable water, including membrane filtration, biological methods, and photocatalytic degradation. The deterioration of these substances is significantly influenced by the oxidation-reduction reaction. The advanced oxidation process involves photocatalytic degradation of dye, which degrades dyes to CO2 and H2O and is hence useful in avoiding water pollution (Babar et al., 2022; Benhadria et al., 2022; Rafique et al., 2020).

For the preparation of metal oxide nanoparticles, several physical and chemical synthesis techniques have been utilized, including electrochemical deposition, ball milling, sol-gel methods, laser ablation, chemical vapor deposition, electrophoretic deposition, thermal evaporation condensation, direct calcination, solution combustion, and hydrothermal processes. We applied the sol-gel process, which is the simplest, least expensive, and fastest of these synthetic methods and may be used to create a wide range of nanomaterial morphologies (Uddin et al., 2020; Liu et al., 2019). In order to create vanadium oxide (V2O5) nanoparticles for the breakdown of methylene blue dyes, this study used ammonium metavanadate and *Laggera tomentosa* leaf extract. It was then determined whether vanadium pentoxide nanoparticles were photocatalytically active by reducing methylene blue (MB). Several techniques were used to characterize the resulting nanoparticles, including X-ray diffraction, UV-visible spectroscopy, Fourier transform infrared, and scanning electron microscopy.

1.2 Statement of the problems

Even in minute concentrations, dyes, the main water pollutants, decolorize the surface of water readily and contribute to pollution. Dyes were extracted from wastewater using some traditional

treatment processes, including chlorination, coagulation, dual-media filtering, and flocculation. Even though they are useless. Because of their remarkable qualities, including a wide and direct bandgap, great thermal stability, high exciton binding energy, and strong catalysis, vanadium oxide (V_2O_5) nanoparticles have grown to be a popular commodity and have grabbed worldwide attention over the years. Due to its affordable cost, environmental friendliness, and readily controllable pathways, the green synthesis technique is the best approach for vanadium oxide (V_2O_5) nanoparticles. Though the synthesis of V_2O_5 using *Laggera tomentosa* plant leaf extract by the sol-gel process has not been reported, there have been reports of green production of V_2O_5 NPs employing many plant extracts. The synthesis of V_2O_5 nanoparticles hence utilized the extracts of *Laggera tomentosa* plant leaves as reducing and capping agents. Ecologically friendly and economically feasible, *Laggera tomentosa* plants lessen the drawbacks of the aforementioned chemical techniques and lower contamination, hence producing sustainable practices. Because of their great thermal photostability, which inhibits biodegradation, organic dyes can endure in the environment for a long time.

1.3 Objectives

1.3.1 General Objective

This study's primary goals were to create and describe vanadium oxide (V_2O_5) NPs using sol-gel techniques and to examine the photocatalytic activity of V_2O_5 for methylene blue (MB) reduction.

1.3.2 Specific Objectives

- To synthesize V_2O_5 NPs from ammonium metavanadate salt by using *Laggera tomentosa* leaf extract.
- To characterize the synthesized V_2O_5 NPs by using XRD, BET, SEM, UV-Vis, and FT-IR.
- To assess the photocatalytic efficiency of V_2O_5 NPs in the removal of methylene blue

1.4 Significance of the Study

The community can learn more about the environmentally friendly manufacture of vanadium oxide (V_2O_5) nanoparticles for the breakdown of methylene blue (MB) dyes from this work. The paper also covered the fundamentals of vanadium oxide (V_2O_5) nanoparticles and how to make

NPs from the *Laggera tomentosa* plant. The study's conclusions can also serve as a springboard for further research in this area for scholars who are interested.

1.5 Scope of the study

The major range of this research work involved the green production of V_2O_5 NPs from its precursor ammonium metavanadate, followed by characterizing the synthesized V_2O_5 NPs by using UV-Vis, BET, FT-IR, XRD, and SEM. Therefore, the disgrace of methylene blue (MB) was examined using the photocatalytic activity of V_2O_5 NPs.

2 LITERATURE REVIEW

2.1 Nanoscience and Nanotechnology

For a century, researchers have been studying nanotechnology. The idea of nanotechnology was initially introduced by 1960 Nobel laureate Richard P. Feynman in his famous lecture "The Plenty of Room at the Bottom" (Richard P. Feynman, 1960). Nanotechnology has seen a number of ground-breaking advancements since then. Materials of various kinds are created by nanotechnology at the nanoscale. A nanoparticle is a particle that is less than 100 nanometers in size (Khan et al., 2017). The word "nano" comes from a Greek word that means "very small." The prefix nano, which denotes a fraction of one billionth (10^{-9}), can be used to refer to length (nanometer), weight (nanogram), volume (nanoliter), or time (nanosecond). In this widespread usage, "nano" means length, and "nanoscale" means a length between about 1 and 100 nm from the atomic level. Currently, nanotechnology is the most important and rapidly growing field of research. Nanotechnology is useful in several areas, such as healthcare, disinfectants, cosmetics, environmental health, chemical industries, and photochemical applications (Demissie et al., 2020). Depending on their standard shape, those substances may be 0D, 1D, 2D, or 3D. The significance of these materials became apparent when scientists discovered that a substance's size can affect its optical and other physicochemical characteristics.

Nanomaterials are an intriguing class of materials that may be highly sought after for a wide range of real-world uses in various industries. Ten hydrogen atoms or five silicon atoms can be used as examples to illustrate the entirety of a nanometer. One nanometer is shown by the covered atoms. Materials that fall between one and one hundred nanometers in length or one of their properties are referred to as nanomaterials. Clarifying the exact records of people's use of nanosized objects is challenging. However, the records of nanomaterial usage are ancient, and humans used those substances long-term in the past for numerous applications, unknowingly. About 4500 years ago, people exploited asbestos nanofibers to reinforce ceramic mixtures. The historical Egyptians have been acquainted with PbS nanoparticles for approximately 4000 years in the past, and used them in a historical hair-dyeing formula (Kammakam, 2021).

The Lycurgus Cup is the oldest known document of nanotechnology. The 4th-century A.D. Roman dichroic cup radiates jade-green under direct light but a ruby-red translucent sheen under backlit illumination. These beautiful optical characteristics are due to the incorporation of silver (Ag) and gold (Au) nanoparticles in the glass matrix. The nanometer was coined as a scientific

word in 1914 by Richard Adolf Zsigmondy. After that, in 1959, Nobel physicist and American physicist Richard Feynman gave his revolutionary lecture, "There's Plenty of Room at the Bottom," before the American Physical Society meeting. While delivering his speech, Feynman came up with the revolutionary idea of engineering and manipulating matter at the atomic and molecular scale. He challenged the question, "Why can't we write the whole 24 volumes of the Encyclopedia Britannica on the head of a pin?" —drawing attention to the fact that what holds back atomic-scale engineering is not disobedience of the laws of nature but merely that no proper tools and techniques exist to achieve it. This lecture is widely held to be the theoretical basis of current nanotechnology, and Feynman is understandably known as its father. It was not until many years later that the term "nanotechnology" was actually coined by Norio Taniguchi in 1974, when he described it as "the processing, separation, consolidation, and deformation of materials by one atom or one molecule." While nanotechnology was still a purely theoretical assumption through the 1980s, these initial results served as the intellectual foundation for its progression into an applied and growing scientific field (Kammakam, 2021).

Nanomaterials are synthesized using two main approaches. Top-down and bottom-up techniques are illustrated in Figure 1. Top-down methods involve the fabrication of nanostructured materials by breaking down bulk materials into smaller structures. Common techniques in this category include mechanical milling, laser ablation, etching, sputtering, and electrical explosion. In contrast, bottom-up approaches rely on the assembly of materials from atomic or molecular precursors. Examples of bottom-up techniques include chemical vapor deposition (CVD), solvothermal and hydrothermal methods, the sol–gel process, soft and hard templating, reverse micelle techniques, and green synthesis (Kammakam, 2021).

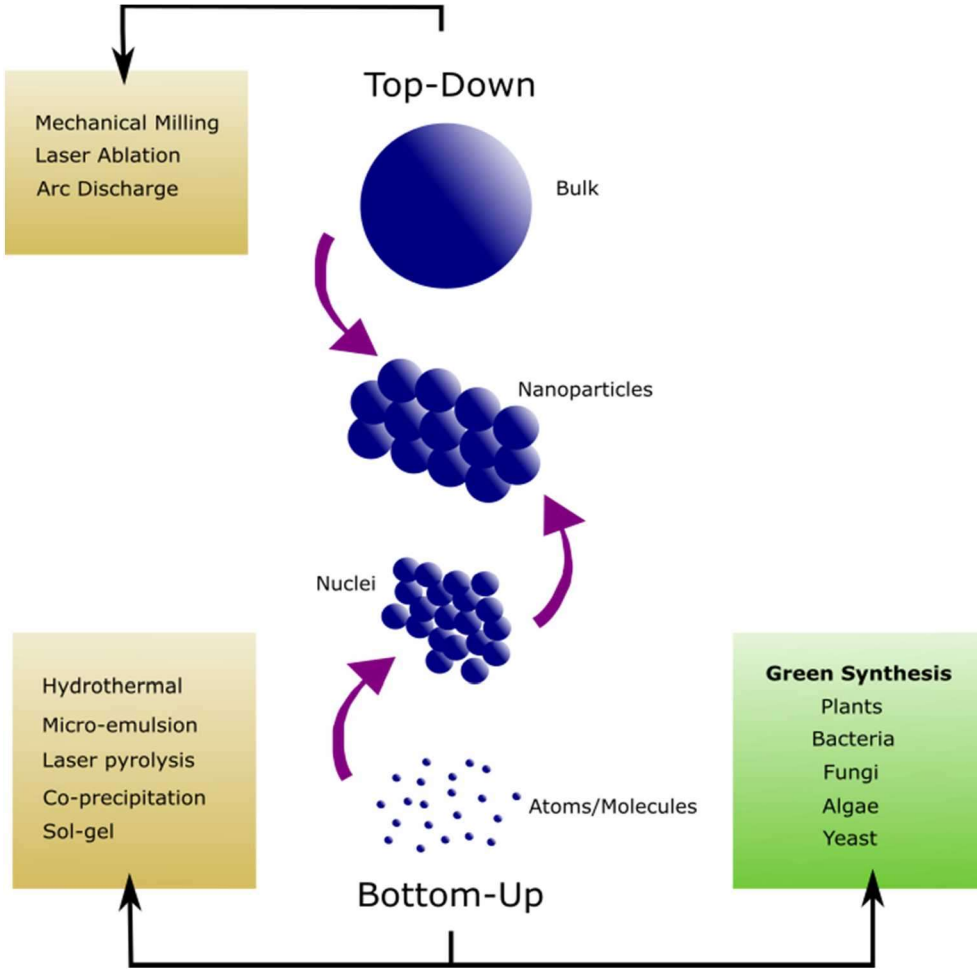

Figure 1**:** Schematic representation of 'top-down' and 'bottom-up' approaches of nanomaterials *(*Drummer *et al.,* 2021).

2.2 Nanomaterials and Nanoparticles

Compared to the massive particles of the mass fabric from which they were made, nanomaterials' size, distribution, and shape provide them with new and more potent advantageous dispositions. Nanomaterials varying in dimension from 1 to 100 nanometers, and their innovative uses in a variety of sectors, including electronic devices, magnetic fields, optoelectronics, along data storage, are expanding quickly due to their improved or new features (Jemal et al., 2017). Nanoparticles have demonstrated significant antimicrobial activity, making them valuable in medicine. Additionally, they are widely used in the fields of cosmetics, biomedicine, medicine, food and feed, pollution control, the mechanics and the chemical sector, semiconductor electronics, aerospace, power science, catalysis, single-electron transistors, light emitters, dynamic optical devices, and various other applications. Among nanomaterials, metallic NPs are particularly promising because of their powerful antimicrobial properties,

especially in the face of increasing microbial resistance to antibiotics. Because of their strong antiviral, antibacterial, antifungal, and anti-inflammatory properties as well as their exceptional conductivity, chemical stability, and catalytic activity, silver nanoparticles distinguish out among heavy-metal nanoparticles. They are being included in electronic components, cryogenic superconducting materials, hybrid fibers, food industry formulas, and cosmetics.

Recent reviews highlight advances in AgNP-based composites to enhance antimicrobial efficacy against antibiotic-resistant bacteria, innovations in green synthesis, and improvements in biocompatibility and delivery strategies (Manisekaran et al., 2024; Khalifa et al., 2025). Because the ratio of atoms on the particle surface to those inside the particle is significantly enhanced, decreasing to such tiny dimensions in the case of nanomaterials may have significant implications for material properties. Differences in surface energies can drive large changes in physical and chemical properties. For example, the redox equilibria and phase stability of a series of metal oxide nanoparticles (M=Co, Fe, Mn, Ni) have been recently reported to strongly depend on the surface energies of the particles (Corr, 2012).

The genus Laggers Sch. Bip. ex Benth. & Hook., which has roughly 20 species and is primarily distributed in sub-Saharan Africa and Southeast Asia, is a member of the Asteraceae plant family. In addition to the aerial parts, the leaves' antiseptic, anti-inflammatory, anti-viral, anti-oxidant, hepatic protective, insecticide, antifungal, anthelmintic, sedative, antituberculosis, and antidiarrheal qualities have been proven. Most of its species are widely utilized by people and conventional medications to treat a variety of conditions, including bacterial infections, irritation, anemia, leukemia, bronchitis, phlegm removal, and more (Getahun et al., 2020).

According to descriptions, Laggera tomentosa Sch. Bip. ex Oliv. Et Hiern is a hairy herb or yearly aromatic foliage that is widely used in Ethiopian traditional medicine. This plant's leaves are frequently used to cure a variety of illnesses, including rabies, leech infestations, pain in the head, dysentery, feverish conditions, and the typical cold, cough, and flu. The aerial parts have historically been used to treat ringworm, toothache, and irritation, while the roots are still used to treat the "evil eye." In addition, the plant has been known to reduce stomach problems, act as a fumigant, ease migraines, and purify milk vessels. It is also used to treat parasite infestations in the extremities and skin infections. Phytochemical investigations reveal that monoterpenes, cyclitols, flavonoids, and sesquiterpenes, including eudesmanes and eremophilanes, are present in significant amounts in L. tomentosa. Flavones, fatty acids and their derivatives, sterols such

as stigmasterol and β-sitosterol, phenolic acid, including 2-hydroxybenzoic acid, and phytotoxic thymol derivatives, such as 3-hydroxythymoquinone and 5-acetoxy-2-hydroxythymol, have also been discovered in the extracts of species of the genus Laggera. Furthermore, the plant extracts commonly contain juniper camphor, γ-eudesmol, 10-epi-?-eudesmol, α-humulene, β-caryophyllene, and 2,5-dimethoxy-p-cymene (Getahun et al., 2020).

2.3 Approaches for the Synthesis of Vanadium Pentoxide Nanoparticles

The process of creating NPs entails atomic-level material customization to achieve special qualities that are completely manipulable for widespread uses. There are three broad nanoparticle synthesis methods for various applications. These are physical, chemical, and natural methods. Depending upon the selected path of synthesis and different experimental conditions, the V_2O_5 NPs of different morphologies, sizes, and shapes can be obtained. In general, V_2O_5 NPs can be obtained by two methods: those are bottom-up and the top-down approach. In the top-down (physical) approach, the size of vanadium metal in its bulk form is reduced mechanically to the nanoscale, utilizing sophisticated methodologies such as laser ablation, thermal decomposition, evaporation-condensation, etc. The self-assembly process is another name for the bottom-up (chemical and biological) method. V_2O_5 NPs are made from their fundamental building blocks, which react to form vanadium oxide nanoparticles with the required size and shape. These components include dissolving vanadium salt in a solvent, reducing vanadium oxide ions to their element by adding a reducing agent, and stabilizing the resulting vanadium oxide nanoparticles with a stabilizing agent to stop them from clumping together.

This section will address different synthesis and preparation conditions and their structural effects on V_2O_5. V_2O_5's adaptability in a variety of synthesis-based applications is an intriguing feature. Sol–gel is the most widely used synthesis process; however, alternative approaches, including electrochemical deposition, chemical vapor deposition (CVD), physical vapor deposition (PVD), hydrothermal/solvothermal synthesis, green synthesis methods, and surfactant-assisted methods, can also be employed. Combinations of these techniques are frequently used to produce various V_2O_5 structures. V_2O_5 can be formed as a powder, nanomaterial, thin film, porous material, etc., by controlling the reaction conditions (Buckner et al., 2016).

2.3.1 Sol–gel Method of Synthesis

The sol-gel synthesis technique is primarily dependent on the condensation and hydrolysis of precursor material. Whenever the ammonium vanadate forerunner was transformed into a heated interior of a platinum crucible, Ditte described this process in 1885 and saw the development of a red sol. Other comparable experiments had been posted a few years later through Blitz. During the sol–gel process, the formation of V_2O_5 occurs during the oxidation and oxolation stages in pH 2 (Figures 2 and 3). In the oxidation process, the V5+ center exhibits hexacoordination. Along the z-axis, a water molecule occupies one position, while an oxygen atom with a double bond is situated on the opposite side. The equatorial plane contains the remaining four bonds, with water and hydroxyl (-OH) groups positioned on opposite sides along the x-axis. Finally, on the y-axis, there are two bonds of -OH on opposite sides. Due to distortion inside the structure, the period of bonds isn't equal, and the discharge of water molecules from the x-axis occurs, resulting in the connection between the V5+ central link with oxygen from the different molecule coordinates forming the oligomer chain polymers. After the oxidation occurs, a reaction in the z-axis is called oxolation.

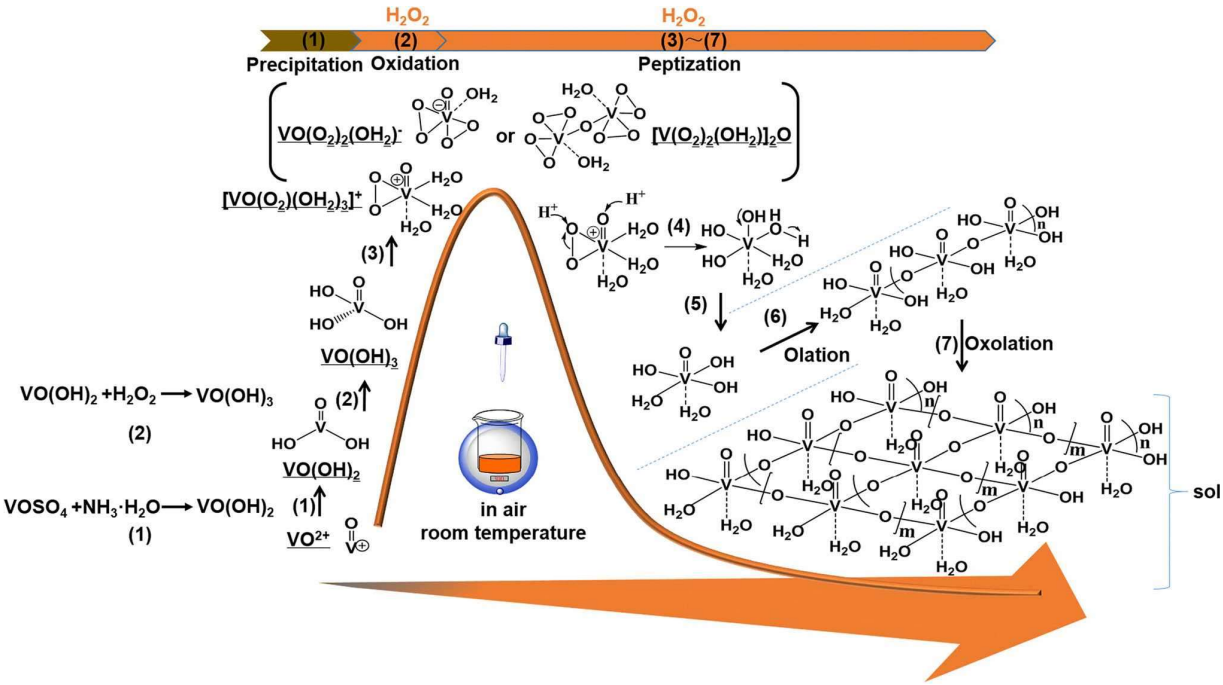

Figure 2: Proposed formation mechanism of V_2O_5 sol at room temperature in air (Li *et al.*, 2017).

Edge-sharing double chains were created along the y-axis as a result of the oxidation. This step involves a condensation process that leads to the synthesis of (-O-V-O′-) n, which is joined with O′ from different coordinates of -O′-V- molecules. Last but not least, the Van der Waals force shapes and connects ordered planes along the y-axis of polymerized VOx. A lamellar shape is being produced by other planes, with an intermediate distance of about 1.17 nm. An interaction response of different materials can be carried out with this interlayer spacing without affecting the crystal structure of V_2O_5 (a topotactic process). New materials produced by intercalation processes have precise or better characteristics (synergistic effect). Sol-gel synthesis produces V_2O_5 with a reddish-brown color and low viscosity. It dries at room temperature to create a thin layer called xerogel. Steady and aqueous levels are distributed throughout each other to create a gel. Initially, a sol is created in this technique by dispersing colloidal particles in a liquid. This sol can be deposited by spinning, spraying, or coating to create a thin layer on any substrate. After the stabilizing components are removed, particles in the sol are allowed to polymerize, further creating a complex network gel. Sol-gel techniques have the advantage of being more cost-effective and achieving a low-temperature procedure that allows us to control the product's composition. The two main processes in this process are condensation and the hydrolysis of alcoholic groups. The steps in sol-gel synthesis are blending, forming, gelation, gel aging, drying, and densification (Mohamed & Shafey, 2020).

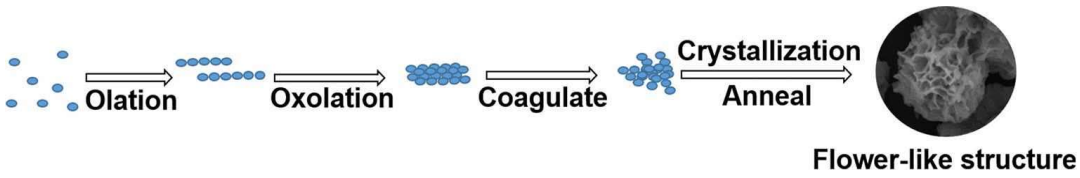

Figure 3: Schematic illustration of the evolution process from sol to flower-like V_2O_5 (Li *et al.*, 2017)

2.3.2 Hydrothermal/Solvothermal Synthesis Method

The processes of hydrothermal and solvothermal synthesis are frequently used to prepare inorganic materials. These techniques are generally carried out in an autoclave, where aqueous (hydrothermal) or non-aqueous (solvothermal) solutions are subjected to high temperatures and pressures. Precisely, the crystalline particle formation by hydrothermal synthesis is dependent on the dissolution of inorganic compounds in hot solutions having a relatively moderate vapor pressure. In vanadium pentoxide (V_2O_5), for example, hydrothermal synthesis using precursors such as ammonium metavanadate (NH_4VO_3) can yield powdered solids containing the

orthorhombic α-V_2O_5 phase, which consists of two-dimensionally layered structures constructed from edge- and corner-sharing VO_5 polyhedra. The polyhedra may further be of various coordination geometries, such as square pyramidal, trigonal bipyramidal, and tetrahedral. Diverse V_2O_5 nanostructures such as nanorods, nanowires, nanotubes, nanobelts, nanosheets, nanoflowers, and hollow spheres are obtained through hydrothermal synthesis through the modulation of reaction conditions such as temperature, pH, and precursor concentration (Sarkar, Das, & Karan, 2022). Porous morphologies such as micro-, meso-, and microporous are also obtained. Besides this, it is demonstrated that the physical properties of V_2O_5 nanoparticles are affected under hydrothermal conditions. For instance, Hussain et al. (2022) illustrated that reaction temperature affects particle size, bandgap, and photocatalytic activity, where smaller particles with greater photocatalytic activity are achieved at lower temperatures. Moreover, sol–gel and hydrothermal hybrid have been revealed to synthesize V_2O_5 with novel structural and morphological characteristics at all scales, thereby enhancing its optical, electrochemical, and photocatalytic activities (Buckner et al., 2016; Farahmandjou, 2017).

2.3.3 Chemical Vapor Deposition (CVD) Synthesis Method

Chemical vapor deposition gives precise control of the composition of deposited films by controlling the chemical precursors and is a very efficient method for depositing nanostructured V_2O_5 thin films. Vapor-phase precursors typically undergo gas-phase and/or substrate surface reactions in CVD. This direct chemical reaction allows for the deposition of materials with excellent uniformity, even over large areas. Some of the many CVD variants include atomic layer deposition (ALD), aerosol-assisted CVD, spray pyrolysis, pulsed-pressure metal-organic CVD, atmospheric pressure CVD, thermally activated CVD (TACVD), plasma-enhanced CVD (PECVD), and photo-initiated CVD (PICVD) (Abuzeid et al., 2021). In general, a vanadium precursor is dissolved or vaporized (possibly with ultrasonic assistance), introduced into a heated reactor, commonly using a carrier gas like N_2, and deposited onto a substrate. After a reaction time (e.g., on the order of one hour), the reactor is cooled to room temperature. The V_2O_5 films deposited are normally bright yellow and adhere strongly to the substrate. The material arrives at the substrate in the form of vapor, gaseous species, or volatilized liquid/solid precursors, which may evaporate, sublimate, or decompose during the process. Recent work using plasma-enhanced atomic layer deposition (ALD), which is a variant of CVD, has demonstrated thin V_2O_5 films (~1-10 nm) with orthorhombic phase appropriate for memristive

applications. These films show typical phase-characteristic Raman modes and distinct memristive switching behavior that depends strongly on film thickness (Buckner et al., 2016b).

2.3.4 Green Synthesis Methods

The generation of metallic nanoparticles by green synthesis is comparatively less studied than the more well-established physical and chemical approaches. In order to create nanoparticles, green synthesis uses biological mediators like algae, fungi, bacteria, and plant extracts. Green nanotechnology is an effective method to minimize harmful effects associated with the production and application of nanomaterials, thereby preventing probable environmental and health risks. Their biomolecules, cells, and tissues can be utilized to create new nanomaterials with environmentally sustainable advantages (Talavera et al., 2013; Din et al., 2017). Green nanotechnology is an innovative catalyst because it enables the development of nanomaterials and products that reduce or eliminate pollution, thereby facilitating the remediation of existing environmental problems. Besides, green synthesis methods preserve inherent characteristics of nanomaterials, for instance, catalytic activity, electrical conductivity, optical sensitivity, magnetic properties, and biological function with certain control over critical parameters like size, shape, surface charge, chemical composition, surface area, and aggregation behavior (Nguyen et al., 2018; Ying et al., 2022).

2.3.4.1 Plant Extract Templated Synthesis Method

Plant extracts' proteins and carbohydrates are essential as reducing agents in metal ion reduction and in the formation of metallic nanoparticles (MNPs). More specifically, proteins and functional amino groups play key roles in the reduction of metal ions. Functional groups such as alkaloids, flavones, and anthracenes –C–O–C–, –C–O–, –C═C–, and –C═O– groups also initiate MNP synthesis. The green process of MNPs and MONPs using plant extracts exhibits varied biological activities like antibacterial, antifungal, anticancer, and larvicidal activities. Seeds, bark, flowers, tubers, and roots of various plants have been used for nanoparticle synthesis, but leaf extracts are the most precious resource for MNPs and MONPs synthesis. This is because leaves are rich in metabolites and, being non-destructive and rejuvenating, unlike other plant tissues, can be harvested, rendering them a sustainable option for the synthesis of nanoparticles (Nguyen et al., 2018; Ahmad & Sharma, 2012).

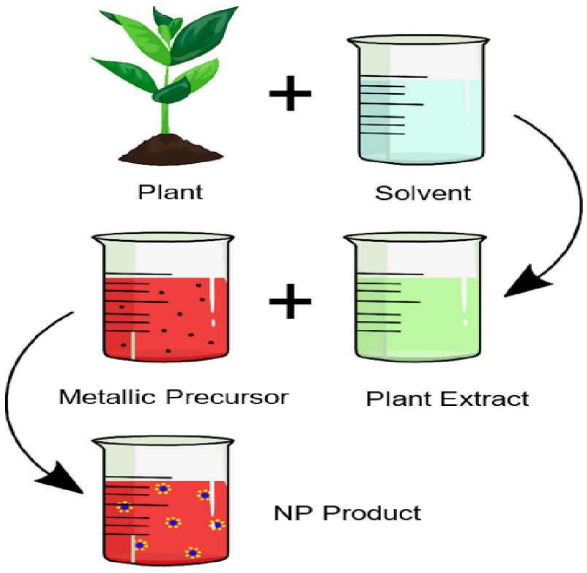

Figure 4: General procedure for acquiring plant extracts for green synthesis of nanoscale material (Drummer *et al*., 2021).

The creation of NPs using bacterial obtains is a green method, but it has several drawbacks, including the time-consuming nature of microbe screening, the need to closely monitor culture medium and the entire process to prevent contamination, the inability to control NP size and shape, and the high cost of the media utilized for growing bacteria. As an example, B. licheniformis generated ecologically safe ZnO nanoflowers that exhibited photocatalytic activity and eliminated the methylene blue dye. It is thought that the enhanced photocatalytic activity of the generated nanoparticles is due to a larger oxygen vacancy. These nanoflowers outperformed other photocatalytic materials in terms of photocatalytic activity (Agarwal et al., 2017).

2.3.4.2 Fungal Extract Assisted Synthesis Method

Fungal extracellular creation of nanoparticles (NPs) has several benefits, such as cost-effectiveness, easy downstream processing, and scalable manufacturing. Due to their capacity for better bioaccumulation and metal tolerance, fungi are selected rather than bacteria. In recent years, fungi in nanotechnology have landed limelight, especially in agriculture and plant disease management. Nanoparticle producers have emerged as major fungi, showing efficiency in the production of intracellular and extracellular MtNPs with uniform size distribution and stability. Fungal-mediated synthesis has the major advantage of producing specific enzymes abundantly, being easily handled in the laboratory, and being scalable and economically feasible at the

industrial level. These features make it ecologically friendly with myco-nanotechnology, cost-effective, and sustainable in nanoparticle production. (Sidhu et al., 2025)

2.3.4.3 Algal Extract Templated Synthesis Method

A class of autotrophic organisms, algae are significant both ecologically and economically. These are organisms with one or more cells that only live-in particular environments, such as freshwater, saltwater, or moist rock surfaces. The two distinct kinds of algae are larger macroalgae and microalgae, which are smaller. Algae-based nanomaterials are very promising due to their widespread applications in the areas of medicine, pharmacy, forestry, aquaculture, and cosmetics. Algae also serve as an important source of industrial products like natural pigments and biofuels. Synthesis using algae-assisted nanoparticles is a branch of nanoscience that has been initiated under the term phyconanotechnology, a new and rapidly developing branch of science. Algae were reported to be highly suitable for nanosynthesis because they possess a high bioaccumulation ability for metals, easy growth, low-temperature growth potential, and environmental friendliness. Various algal classes, such as Chlorophyceae, Phaeophyceae, Cyanophyceae, and Rhodophyceae, are utilized most commonly for synthesizing silver, gold, and other metal and metal oxide nanoparticles (Sajid et al., 2020). Physicochemical properties of the obtained nanoparticles, i.e., size, shape, and stability, are a function of temperature, pH, metal ion concentration, exposure time, and reducing agent type and concentration in the reaction medium. Metal ion reduction to nanodimensional particles occurs on the algae cell surface in extracellular synthesis, whereas intracellular synthesis involves enzymatic activity for reduction within the cell membrane and cytoplasm. Among the various methods, the utilization of live cultures of algae is one of the simplest and most effective methods of nanoparticle biosynthesis (Zhang et al., 2021).

2.3.5 Surfactant-Assisted Synthesis Method

V_2O_5 nanostructures are made with a surfactant. The resulting nanomaterials are surfactant aggregates that are nanometers in size and contain water molecules that are contained within the solvent. Anionic, cationic, zwitterionic, nonionic, and mixed surfactants were among the several types of surfactants that were utilized. The water concentration, represented by mol [water]/mol [surfactant], regulated the nanoscale size. A sol-gel method assisted by surfactants was used to produce V_2O_5 NPs (Vo et al., 2018). Characterization of Vanadium Oxide V_2O_5 NPs.

2.4 Characterization techniques

To identify and control the manufacturing and applications of nanoparticles, characterization is essential. A nanoparticle's potential and use are determined by its distinct properties. These attributes include concentration, crystallography, surface area, size, composition, surface shape, and surface charge. In order to determine the phase purity, size, shape, form, structure, atomic surroundings, surface charge, etc., vanadium pentoxide nanoparticle characterization is essential. Through the use of sophisticated analytical methods, including scanning electron microscopy (SEM), ultraviolet-visible spec (UV-vis spectroscopy), infrared spectroscopy (FTIR), and X-ray diffraction (XRD).

2.4.1 UV-Vis Characterization of Vanadium Oxide (V_2O_5) Materials and Methods

Ultraviolet-visible spectroscopy (UV-Vis) is a technique that investigates the behavior of photons in interaction with matter within the ultraviolet and visible regions of the electromagnetic spectrum. UV-Vis applies light within the near-ultraviolet (UV), visible, and near-infrared (NIR) ranges to probe electronic molecule transitions. Ultraviolet-visible spectrophotometers are usually employed to measure the absorption or transmission of light in liquids and in transparent or semi-transparent solids. Typically, these instruments operate in the wavelength range 200–800 nm in order to detect electronic transitions characteristic of different chemical bonds and molecular forms. Wavelengths below 200 nm are usually avoided because oxygen absorbs very strongly in this region, and thus, accurate measurements are not feasible. Upon a sample being passed through by light, some wavelengths are absorbed based on the molecular content in order to obtain useful information about the structure and properties of the sample. (Kruefu et al., 2017).

2.4.2 FT-IR Characterization of Vanadium Oxide (V_2O_5)

FT-IR was used for determining the presence of potential biomolecules, chemical composition, and functional groups of nanoparticles. Chemical bonds and functional groups in the molecule were identified by the synthetic V_2O_5 nanoparticles' infrared spectrum (FT-IR), which fell between 400 and 4000 cm^{-1} wave number. For the O-H and C-H groups, the wide bands at 3135 cm^{-1} and 3037 cm^{-1} are responsible. It is the bent vibrations of the C=C vibration that cause the absorption peak at 1401 cm^{-1}. The V=O vibrations at 967 cm^{-1}, the V-O-V symmetric stretch at about 531 cm^{-1}, and the V-O-V asymmetric stretch at 730 cm^{-1} were the three distinctive vibration modes visible in the FTIR spectra of V_2O_5 nanoparticles (Baudot et al., 2010).

2.4.3 XRD Characterization of Vanadium Oxide (V_2O_5)

A nondestructive analytical method called X-ray diffraction (XRD) may reveal important details about the lattice framework of a crystalline material, including the size of the unit cells, bond angles, chemical makeup, and crystallographic structure of both natural and artificial materials. The foundation of XRD is the idea that a crystalline sample and X-rays can interfere constructively. The crystalline phase and crystalline size were determined using an X-ray diffractometer (XRD). XRD was used to structurally characterize the V_2O_5 nanoparticles (Whitfield & Mitchell, 2004).

2.4.4 SEM Characterization of Vanadium Oxide (V_2O_5)

SEM methods generate compositional data and topography image data as the electron beam interacts with the sample. Conductivity is a prerequisite for SEM analysis. Ion sputtering or vacuum evaporation are two methods used to cover insulator samples with carbon or a metal. Applying a conductive covering to the sample reduces thermal damage, stops the sample from charging, and improves the SE electronic signals. V_2O_5 nanoparticles were morphologically studied and described using a field-emission scanning electron microscope (SEM). The surface morphological studies of as-prepared V_2O_5 were examined using SEM.

Table 1: Characterization techniques and determining characteristics of nanoparticles.

S.No.	Characterization techniques	Determined characteristics
1	Ultraviolet-visible spectroscopy (UV-vis)	Concentration and shape of NPs
2	Fourier transform infrared spectroscopy (FT-IR)	Nature of bonds and functional groups
3	X-ray diffraction (XRD)	Size and crystallinity of NPs
4	Scanning electron microscopy (SEM)	Shape, size, and structure of NPs
5	Brunauer–Emmett–Teller (BET)	Specific surface area

2.5 Application of Vanadium Oxide (V_2O_5) Nanoparticles

Vanadium pentoxide (V_2O_5), a material with unique physical, chemical, and structural features that increase its surface-to-volume ratio, has garnered a lot of interest at the nanoscale. With a broad band gap (Eg) of 2.2–2.3 eV, it is an n-type semiconducting material with the most stable oxide and intriguing photocatalysis and electrochemical capabilities. By employing V_2O_5, polluting dyes are degraded, and aldehydes are halogenated through decarbonylative methods.

Lewis's base in V_2O_5 nanoparticles is represented by oxygen atoms with a single pair of electrons and HOMO character, whereas the non-bonded d-orbitals of V ions have LUMO character and serve as Lewis's acid. V_2O_5 nanoparticles have improved photocatalytic activity, microbiological activity (anti-fungal and anti-bacterial), and magnetic properties. V_2O_5 experiences both its transition phase and an oxide crystal structure shift at 257 °C, which modifies optical and electrical properties. It is well known that the size and form of distinct nanomaterials affect their unique capabilities.

2.5.1 Vanadium Oxide (V_2O_5) Nanoparticle for Catalytic Activity

Industrial water constantly incorporates organic-inorganic pollution of poisonous and carcinogenic character. Because of their excessive solubility and stability, hexavalent chromium ions are one of the predominant and distinctively risky pollutants present in wastewaters. In addition, synthetic natural molecules (consisting of dyes and antibiotics), which can be normally utilized in everyday lives and are discharged into water bodies without proper treatment, can cause water pollution. As the demand for easy water is still outstanding across the world, there may be increased interest in green photocatalysts. Photocatalysis generates active species by absorption of light, which degrades the organic waste material and thus can be used as an effective bioremediation tool. These substances may activate the use of solar power for pollutant elimination via oxidation or reduction. Aside from the course of synthesizing new materials, a similarly promising course is the research into the optimized Synthesis of substances for appreciably improving their catalytic properties. Although it is frequently used in photocatalysis, titanium dioxide only absorbs ultraviolet light and exhibits little activity in reactions involving the creation or reduction of oxygen. V_2O is one such substance that shows promise. Research into the effectiveness of V_2O_5 as a bifunctional photocatalyst, capable of catalyzing each oxidation and discount reactions, has been enormously uncommon.

The structure of supported vanadium oxide species, as well as their turnover frequency (i.e., the activity per vanadyl (V=O) site), is strongly influenced by the nature of the support. This relationship has been extensively documented in catalytic studies (Wachs, 2013). In the hydrated state, the structure of supported vanadium oxide species can be inferred from the aqueous-phase chemistry of polyvanadates, with the point of zero charge (pzc) of the oxide support rather than the solution pH determining the species formed. Consequently, supported vanadium oxide species tend to be smaller on basic supports compared to acidic supports. The

size quantization effect of small vanadium oxide moieties increases the energy gap between the highest occupied and lowest unoccupied electronic states relative to bulk V_2O_5, which typically has a band gap of ~2.3 eV. This phenomenon leads to a blueshift in the absorption edge, in extreme cases extending into the UV region for isolated VO_4 monovanadate sites. Although this shift may reduce visible-light absorption, it simultaneously enhances the oxidative and reductive potentials of photogenerated holes and electrons, respectively, thereby enabling photocatalytic reactions that are not feasible with bulk crystalline V_2O_5. This process is often described as band-gap engineering (Kortewille et al., 2022).

2.5.2 Vanadium Oxide (V_2O_5) Nanoparticle for Photocatalytic Degradation of Organic Pollutant Dyes

The use of semiconductor photocatalysts in advanced oxidation processes (AOPs) for the removal of organic pollutants has become a popular pastime in recent years. A wide range of natural contaminants can be quickly and nonselectively oxidized by highly reactive species like hydroxyl radicals produced in AOPs. Due to their precise strengths for fully mineralizing organic contaminants into less hazardous byproducts, including water, CO_2, and mineral acids, semiconductor photocatalysts are widely used. Because of the nanoparticles' broad bandgap, researchers have often employed them as UV-induced photocatalysts to break down organic molecules and contaminants. In theory, semiconductor photocatalysts could significantly improve the decomposition efficiency of organic molecules under visible light irradiation. To create semiconductor photocatalysts powered by visible light, a number of approaches have been investigated. Additionally, vanadium dioxide (VO_2) nanoparticles and other semiconductors with narrow band gaps may be employed as visible light-driven photocatalysts. A semiconductor driven by visible light, vanadium pent (V_2O_5) nanoparticles were chosen to grow on a flexible substrate, such as a PET fiber, because of its low band gap (2.52 eV). The photocatalytic activities of V_2O_5 nanoparticles in the degradation of methylene blue dye ($C_{16}H_{18}ClN_3S$) under dark and visible light irradiation (Sajid et al., 2020).

The limited quantity of free radicals formed by V_2O_5 only the photogenerated holes could produce free radicals was probably the cause of the decreased photodegradation efficiency.

Consider the following equations:

$$V_2O_5 + h\mathrm{V} \rightarrow h{+}\mathrm{V}b + e\text{-}c \quad \ldots\ldots 1$$

$$h{+}\mathrm{V}b + H_2O \rightarrow H{+} + OH\cdot \quad \ldots\ldots 2$$

$$MB\ dye + O_2^{\cdot -} + OH^{\cdot} \rightarrow byproducts \quad \ldots\ldots\ldots\ldots\ldots\ldots\ldots\ldots\ldots\ldots\ldots\ldots\ldots\ldots\ldots\ldots 3$$

2.5.3 Photocatalytic MB Dye Degradation Activity Studies

To perform the photo-catalytic dye degradation application, MB dye was utilized as a model reaction. Prepared V_2O_5 was employed as a photocatalyst in this instance, and the degradation application was studied using 5 ppm, 10 ppm, and 15 ppm MB solutions that were made from a stock solution. For self-degradation, the produced dye was stored in an area that was both dark and bright; finally, it halted and was prepared for degradation. In the dye solution, a tiny quantity of V_2O_5 powder (20, 30, and 40 mg) was sonicated into uniformity. Dispersed V_2O_5 powder begins to break down MB. One can use equation (4) to compute the catalytic breakdown of dye by a catalyst.

$$\text{Degradation percentage (R\%)} = \frac{Co - Ct)}{Co} \times 100 \quad \ldots\ldots\ldots\ldots\ldots\ldots\ldots\ldots 4$$

Where Co is the initial concentration of dye and Ct is the concentration of dye after time t (Babar et al., 2022, Basfer et al., 2021). The adsorption capacity (qt) of the MB dye onto nanoparticles was calculated through equation (6):

$$\text{Adsorption capacity (qt)} = \frac{Co - Ct)V}{W} \quad \ldots\ldots\ldots\ldots\ldots\ldots\ldots\ldots\ldots\ldots\ldots\ldots\ldots\ldots 5$$

Where W indicates the weight in grams of nanoparticles and V indicates the volume of dye solution in milliliters (Hassan & Rasheed, 2021).

1. **Adsorption isotherms.**

The relationship among adsorbent materials and contaminants is described by stability relationships called adsorption isotherms. These important occurrences express the adsorbent's surface characteristics and capability. Adsorption isotherms are employed to effectively build adsorption systems and optimize the adsorption mechanism. To ascertain the equilibrium correlation between the adsorbent and the adsorbate, adsorption isotherm models are frequently used (Fito et al., 2023; Saad et al., 2021). The most often used adsorption isotherm models are Dubinin-Radushkevich, Temkin, Toth, Freundlich, and Langmuir. The current work examined equilibrium adsorption isotherm models under constant ideal circumstances of contact time (60 min.) and adsorbent dose (20 mg/L) while altering the starting MB concentration (Fito et al.,

2023). Monolayer adsorption on a homogeneous surface is assumed by the Langmuir isotherm model.

The general expression of the Langmuir adsorption isotherm is given in Equation (6), while its linearized form is presented in Equation (7).

$$q_e = \frac{K_L q_{max} C_e}{1+K_L C_e} \quad \text{.....6}$$

$$\frac{1}{q_e} = \frac{1}{q_{max}} + \frac{1}{K_L q_{max} C_e} \quad \text{.....7}$$

It is possible to evaluate the isothermal feasibility of Langmuir using the infinite separation factor constant (RL).

$$R_L = \frac{1}{1+K_L C_e} \quad \text{.....8}$$

Where KL (L/mg) refers to the Langmuir constant related to the free energy of adsorption, whereas qmax (mg/g) is the maximum monolayer adsorption capacity of the adsorbent.

The Freundlich isotherm model, whereby implies the adsorption process occurs on a heterogeneous surface, is one of the most popular adsorption isotherm models. However, the adsorption process is multilayer in nature in the Freundlich adsorption isotherm model.

The Freundlich isotherm model's general equation is given by equation (9), and the linearized form is shown in equation (10) (Fito et al., 2023).

$$q_e = K_F C_e^{\,1/n} \quad \text{.....9}$$

$$\log q_e = \log K_F + {}^{1}/_{n} \log C_e \quad \text{.....10}$$

KF denotes adsorption capacity (mg/g), and 1/n denotes an empirical parameter related to adsorption intensity, with a value between 0 and 1 denoting favorable conditions.

2. Adsorption kinetics.

The velocity at which a substance remains in or is discharged from an aqueous solution to a solid-phase interface for a specific adsorbent dose, ambient temperature, velocity of flow, and

pH level is shown by an adsorption kinetics curve. The kinetics analysis is crucial. It provides data like the solute absorption rate, which is utilized to determine how long the adsorption process will take to complete. Intraparticle diffusion, pseudo-first-order, and pseudo-second-order adsorption kinetic models are well-known. In the current study, a set quantity of adsorbent (20 mg/100 mL), a starting point MB content of 5 mg/L, and various contact times of 0, 20, 40, and 60 minutes were used to investigate adsorption kinetics. The kinetic models, i.e., pseudo-first-order and pseudo-second-order, are presented by Eqs. (11) and (12).

$$\log(q_e - q_t) = \log qe - {}^{K_1 t}/_{2.303} \quad \text{.....11}$$

The plot of t vs. log (qe − qt) results in a slope of − K1t/2.303 and an intercept of log (qe). Similarly, in the pseudo-second-order kinetics, the slope becomes 1/qe, and the intercept will be 1/k2qe2 as t/qt is plotted against (Fito et al., 2023).

$$\frac{t}{q_t} = (1|q_e)t + {}^{1}/_{K_2 {q_e}^2} \quad \text{.....12}$$

A. Effect of dye concentration

The initial number of dyes that can be efficiently destroyed using synthesized nanoparticles has been estimated through experiments conducted for a range of dye solution concentrations. This is because the catalyst's surface area becomes limited as the concentration rises, which lowers the catalyst-reactant ratio. Consequently, dye removal rates have dropped (Shanker et al., 2016).

B. Effect of contact time

The effect of contact duration on photocatalytic degradation of MB dye was investigated under the optimal condition of an initial dye concentration of 5 mg/L. A fixed concentration of 20 mg/L V_2O_5 catalyst was utilized. The link between photocatalytic MB degradation and catalyst contact time was examined. Figure 8 illustrates the results. The degradation of MB has been seen to rise as the catalyst's irradiation period increases. The graph shows that, from zero to 60 minutes, the degradation rate is faster due to the availability of a large number of active sites, and subsequently it reaches equilibrium. The amount of dye degradation reached its maximum as time passed; thereafter, it stayed virtually constant (Saad et al., 2021). This is because, as time increased, the contact time between dye molecules and catalysts increased, speeding up the

breakdown process. The catalyst's active sites will be more available for dye molecules to react at first, but after a while, the catalyst surface will become saturated due to the adsorption of more dye molecules. As a result, increased duration does not affect dye degradation (Fito et al., 2023).

C. Effect of catalyst dosage

One of the key process variables that directly influences the photocatalytic activity is the photocatalyst loading. The efficiency of pollutants' photocatalytic degradation will rise with an increase in catalyst loading. Since larger active sites on the catalyst surface were in charge, more reactive radicals were produced, which improved the photocatalytic destruction of pollutants with the photocatalyst dosage. However, the performance of photocatalytic degradation may be negatively impacted by excessive catalyst loading (Saad et al., 2021). A surplus of photocatalyst will increase the catalyst's aggregation, which will reduce the number of active sites and cause reactive radicals to be produced. Furthermore, in addition to the extreme turbidity of the solution scattering light, an excess of the catalyst will reduce the intensity of light that reaches the aqueous solution. The probable purpose may be that because the dose increases, the range of active sites on the catalyst penetrated through photons receives a block, thereby lowering the inside charge of removal of dyes that had been found (Shanker et al., 2016)

3 MATERIALS AND METHODS

3.1 Chemicals and Materials

All the reagents and chemicals utilized for the synthesis of vanadium oxide (V_2O_5) nanoparticles were analytical grade and purchased commercially from local chemical markets. Ammonium meta-vanadate (NH_4VO_3, CAS 7803-55-6, 99.0+% pure), distilled and tap water (H_2O), ethanol (CH_3CH_2OH), hydrochloric acid (HCl), and methylene blue. Distilled water was used to prepare all aqueous solutions. Those reagents are brought commercially from chemical markets.

The apparatus and instruments that were used during this research include a pipette, furnace, oven, aluminum foil, spatula, test tube with a test-tube rack, electronic beam balance, electrical grinding machine, beaker, magnetic stirrer with hot plate, petri dish, conical flask, volumetric flask, funnels, measuring cylinder, vials, mechanical shaker, Erlenmeyer flask, refrigerator, crucible, mortar and pestle, dropper, and centrifuge. XRD, FTIR, SEM, BET, and UV-vis instruments were used for this study.

3.2 Synthesis of Vanadium Oxide (V_2O_5)

3.2.1 Collection of plant material and preparation of extract

Fresh leaves of *Laggera tomentosa* were collected from Daletti, approximately 26 km southwest of Addis Ababa, Ethiopia, near the Alemgena town. The plant was taxonomically identified and authenticated by the Department of Applied Biology, Adama Science and Technology University. The collected leaves were washed with clean deionized water and cut into small pieces. To make the extract, 5 g of the plant was boiled in 100 mL of ethanol for 5 minutes in an Erlenmeyer flask, and a green-colored solution was collected. The solution was filtered with Whatman filter paper to obtain a clear filtrate, which was kept at 4 °C and utilized within one week. This extract served as a reducing agent and stabilizing agent during vanadium oxide nanoparticle synthesis (Aliyu et al., 2017).

3.2.2 Sol-gel synthesis of vanadium oxide (V_2O_5) nanoparticles

1.17 g and 0.4 mole of ammonium metavanadate were dissolved in 100 mL of distilled water after adding HCl to set the pH to 2.5. The produced extract of Laggera tomentosa plant leaves was then added drop by drop while being stirred at 60 °C. The gel was created by mild heating, resulting in a color change from white to dark green. The dried dark green xerogel (intermediate product) was calcined under vacuum at 450°C for 5 hours to eliminate moisture and precursor material impurities (Abuzeid et al., 2021).

3.3 Characterization of Vanadium Oxide (V_2O_5) Nanoparticles

3.3.1 UV-Vis (Diffuse Reflectance Mode) Spectrophotometer

The UV-Vis (Diffuse reflectance mode) Spectrophotometer was used to verify the formation and balance of vanadium oxide (V_2O_5) nanoparticles. Vanadium Oxide (V_2O_5) nanoparticle powder samples were used periodically to observe the optical reflectance of the sample at the wavelength range from 200 to 800 nm at room temperature, operated at a resolution of 1 nm. The bandgap energy of the produced vanadium oxide (V_2O_5) nanoparticles was calculated using the samples' reflectance spectra. Initially, the reflectance of the powders was measured at Kubelka-Munk (K-M) units. Equations 13–14 below serve as the foundation for the application of the K-M method.

$$[F(R)hv]^n = A(hv - Eg) \quad \text{.....13}$$

$$(R) = 1 - R^2/2R \quad \text{.....14}$$

With R standing for reflectance, Eg for the energy band gap, α for the coefficient of absorption, h for the Planck constant, ν for frequency, A for a constant, and n = 1/2, the band gap energy can be obtained by applying the K-M method to extend the linear region of the spectrum (F(R) hv) 1/2 vs. hv. When the examined samples show excessive absorption or light scattering, this method is commonly employed (Babar et al., 2020).

3.3.2 X-ray diffraction (XRD)

X-ray diffraction equipment (Tokyo, Japan Shimadzu Maxima-7000 model) was used to research the structural properties of V_2O_5 NP powders by producing CuKα monochromatic radiation or an X-ray wavelength (λ=1.5406˚). Phase of quartz, crystalline size, lattice spacing, density of instability, and number of unit cells of crystals in the materials thus produced were all determined by adopting the above procedure. The X-ray machine was run at room temperature with a voltage of 40 kV and a current of 30 mA. At a scan rate of 3°/minute for 2θ between 10° to 80° in continuous mode scanning, XRD intensity was measured in scan steps of 0.0020° per 2θ per second. Structure and crystallinity of synthesized Vanadium Oxide (V_2O_5) nanoparticles were calculated using Debye-Scherrer's equations.

$$D = \frac{K\lambda}{\beta \cos} \quad \text{.....15}$$

The average crystalline size of synthesized nanoparticles was calculated using Scherrer's equations, where D is crystallite size in nanometers, k is the shape factor constant (0.89), β is full width at half maximum (FWHM) in radians, λ is the X-ray wavelength, and θ is the Bragg angle. (Babar et al. 2020).

3.3.3 Brunauer–Emmett–Teller (BET)

Utilizing BET, the specific surface area of the V_2O_5 NPs was determined. Surface area measurement device with instrument specifications: Using the SA-9600 Series from Horiba, the exact surface area of the adsorbent was determined. The instrument was run in a degassing state at 300 °C for an hour in order to conduct this study. Using nitrogen gas adsorption and desorption isotherms at 700 mmHg air pressure and a surface area analyzer, the surface area was determined. Liquid nitrogen was injected at 27.0 °C to improve N_2 adsorption on the surface of the adsorbent. The p/p_0 ratio was utilized to measure the adsorbent's BET-specific surface area (Fito et al., 2023; Munir et al., 2020)

3.3.4 Fourier Transform Infrared (FT-IR) Analysis

FT-IR spectroscopy (FT-IR-6600, model A, Jasco Company, Japan) was utilized to identify functional groups in Vanadium Oxide (V_2O_5) nanoparticle production. V_2O_5NPs were purified with the aid of repeated centrifugation thrice at 18000 rpm for 30 min. FT-IR evaluation of the dried powder of V_2O_5 NPs by means of scanning with potassium bromide (KBr) pellets because of its transparency in the IR, between 400 and 4000 at a resolution of 1 cm^{-1}. The unique peaks in the IR spectrum were interpreted for the exceptional functional group within the formulations, and the main statistics obtained from the IR were recorded (Munir et al., 2020).

3.3.5 SEM Analysis

Scanning electron microscopy (SEM) characterisation was performed to ascertain the size, surface appearance, and form of the reduced vanadium oxide nanoparticles by using a JCM-6000plus Benchtop SEM (SHIMADZU Corporation, Japan) (Kruefu et al., 2017).

3.3.6 Photocatalytic degradation experiment

A photocatalytic reactor was utilized to assess the effectiveness of V_2O_5 nanoparticle degradation. A cylindrical Pyrex glass cell with a volume of 1.0 L, dimensions of 10 cm in

diameter and 15 cm in height, made up the reactor. Employing a 150 W mercury lamp (400–700 nm), the radiation was applied inside a quartz cuvette that was 1 cm wide and sealed with a Teflon stopper. After the cuvette and light were placed in the reactor 3.0 cm from the solution, the system cooled the water to a steady 25 °C. By dispersing methylene blue (MB) in 100 milliliters of distilled water with a pH of 7, a dye stock solution was created.10 mL of the solution was mixed with V_2O_5 nanoparticles to perform photocatalytic tests. The rest of the dye solutions for 5, 10, and 15 mg/L concentrations were obtained by diluting the stock solution with deionized water (Kruefu et al., 2017). Suspension was kept under continuous agitation using a magnetic stirrer throughout the irradiation process to avoid the aggregation of the catalyst and ensure homogeneous dispersion. The photocatalytic activity of as-synthesized V_2O_5 nanoparticles was verified by measuring the residual concentration of MB through a UV–Vis spectrophotometer (OPTIMA SP-3000 Plus, SHIMADZU Corporation, Japan). MB exhibits a characteristic maximum absorbance at λmax = 664 nm, and the degradation efficiency was evaluated based on the decrease in absorbance intensity at this wavelength following exposure to visible light. The percentage degradation efficiency of the catalyst was calculated using Equation (4) (Fito et al., 2023).

4 RESULT AND DISCUSSION

4.1 Spectrophotometry Analysis

Figure 5 illustrates V_2O_5 NPs' diffuse reflectance spectra obtained between 340–800 nm. A reflection peak was viewed at 640 nm, which can be attributed to the oxygen-vanadium charge transfer transition. The optical band gap was derived from a Tauc plot of $(\alpha h\nu)^{1/2}$ vs. photon energy ($h\nu$), as displayed in Figure 5(b). From UV-Vis analysis, the band gap of the synthesised V_2O_5 nanoparticles was found to be 2.94 eV by the relation $Eg(eV)=1240/\lambda(nm)$. This is higher compared to that of bulk V_2O_5 (~2.3 eV) (Wachs, 2013; Kanna & Wongnawa, 2008), which reflects the presence of a quantum size effect due to the nanoscale character of the particles, leading to a blue shift of the absorption edge (Babar et al., 2020).

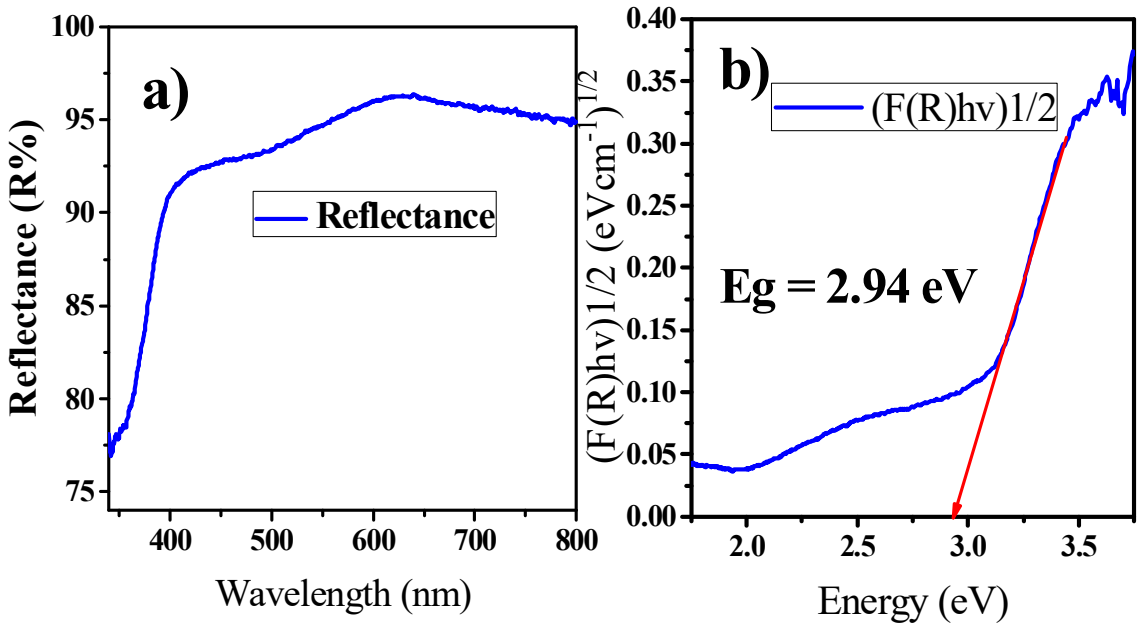

Figure 5: (a) Uv–Vis diffuse reflectance spectra and (b) Tauc plots of $(\alpha h\nu)^{1/2}$ vs photon energy ($h\nu$) for V_2O_5 NPs.

4.2 X-ray diffraction (XRD)

To ascertain the crystal's size and crystalline phase, an X-ray diffractometer (XRD) was used. The V_2O_5 nanoparticles' XRD pattern is displayed in Figure 6. The image indicates strong diffraction peaks existed at 2θ = 15.4°, 20.33°, 21.74°, 26.20°, 31.06°, 32.4°, 34.34°, 41.26°, 45.46°, 47.38°, 48.84°, 51.22°, 55.68°, 59°, 61.14°, 62.12°, 64.58°, 66.06°, 68.84°, 69.62°,

72.3°, 74.5°, 76.02°, and 78.14°, which corresponded to the (200), (001), (101), (201), (110), (301), or (400), (011), (111), (310), (002), (102), (411), (600), (020), or (212), (604), (611), (412), (701), (321), or (420), (710), (103), (711), (303), and (701) crystal planes and as indexed in the JCPDS card number 00- 04-1426, representing the orthorhombic crystalline phase of vanadium oxide nanoparticles. The interlayer spacing (d) values were calculated to be 2.21 Å for the samples, which corresponds to V_2O_5 (Kruefu et al., 2017).

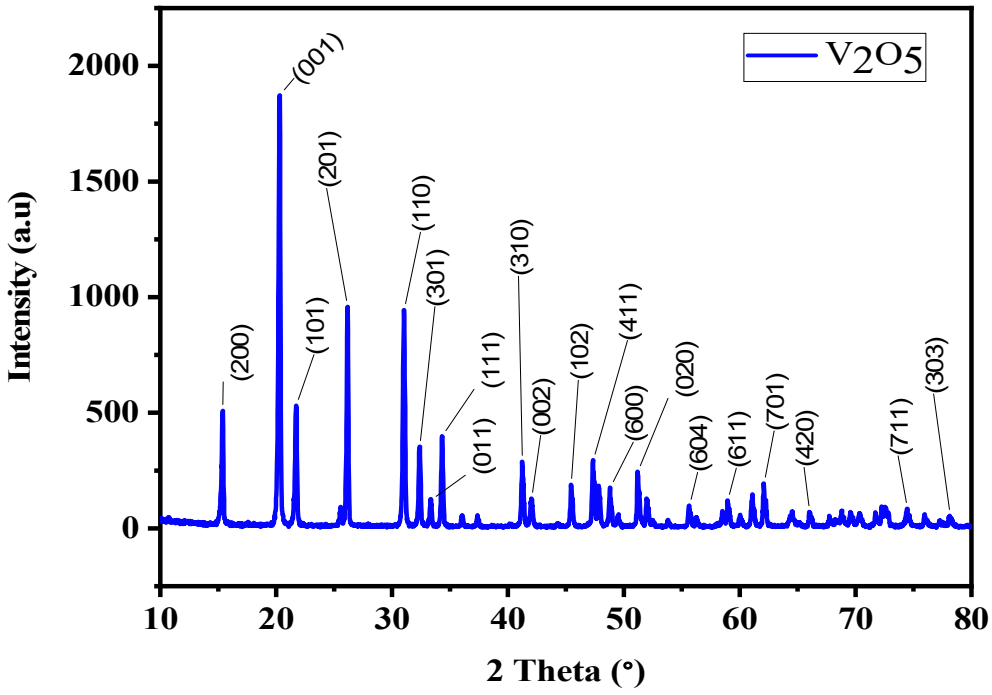

Figure 6: X-ray diffraction patterns of V_2O_5 nanoparticles synthesized using the plant extract.

4.3 FT-IR Analysis

The presence of potential biomolecules, the chemical composition, and the functional groups of nanoparticles were assessed using FT-IR. Figure **7** shows the FT-IR spectrum of the V_2O_5 nanoparticle and the extracted plant. The FT-IR spectra of the produced V_2O_5 nanoparticles were analyzed in the wavenumber range of 400–4000 cm^{-1}, revealing the compound's chemical bonds and functional groups. The O-H and C-H groups are responsible for the huge broad bands at 3015.05672 cm^{-1} and 1744.59746 cm^{-1}, respectively. The bending vibration of the C=C vibration is the cause of the absorption peak at 1367.1666 cm^{-1}. Three distinct vibrational modes were visible in the FTIR spectra of V_2O_5 nanoparticles: V=O vibrations at 1215.52026 cm^{-1} and

1009.95524 cm^{-1}, the V-O-V symmetric stretch at 426.95935 cm^{-1}, and the V-O-V asymmetric stretch at 807.76013 cm^{-1} (Munir et al., 2020).

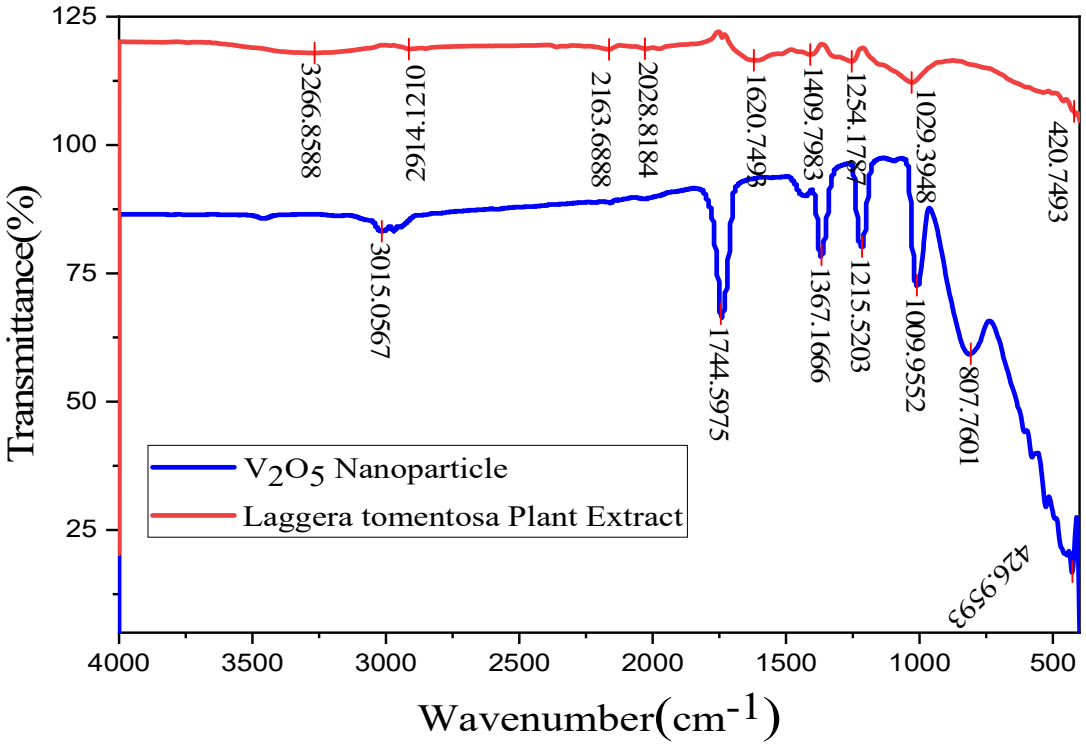

Figure 7: FTIR spectrum of V_2O_5 nanoparticle

4.4 Morphological and Structural Analysis

Scanning electron microscopy (SEM) was used to examine the morphology of nanoparticles of V_2O_5. The JCM-6000Plus machine was used to analyze the surface morphological studies of the prepared V_2O_5. Figures 8(a), 8(b), and 8(c) show the images of V_2O_5 nanoparticles with various magnifications. The catalyst's surface structure was discovered to be an aggregation of particles of varied sizes. SEM micrographs show porous agglomerated clusters with fine voids in the structure. SEM images revealed that V_2O_5 particles are distributed randomly in irregular flake-like morphologies and have a good crystalline morphology of nanoparticles (Fito et al., 2023).

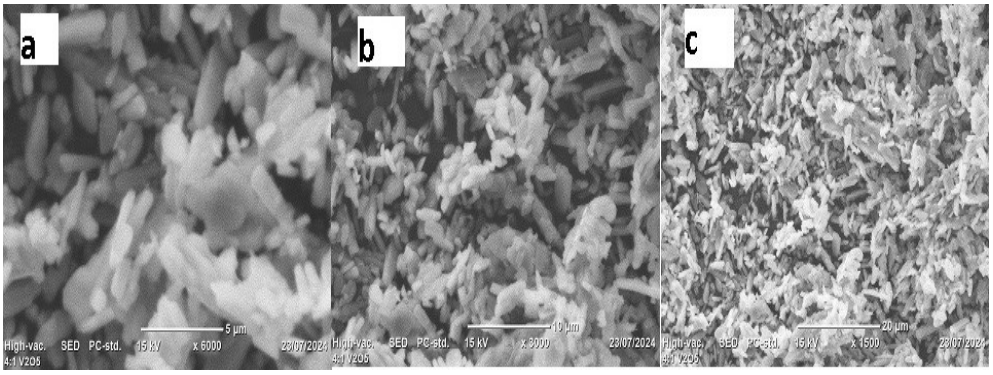

Figure 8: SEM images of V_2O_5 nanoparticles at various magnifications.

4.5 Brunauer–Emmett–Teller (BET)

The specific surface area of the generated adsorbent was determined using BET. For this investigation, the machine was operated at the degassing temperature of 300°C for an hour. Utilizing a surface area analyser and nitrogen gas adsorption and desorption isotherms at 700 mm at atmospheric pressure, the surface area was calculated. The adsorbent's surface was coated with liquid nitrogen at 27.0°C to improve N_2 adsorption. Using the p/p_0 ratio, the BET-specific surface area of the V_2O_5 nanoparticles is determined in Figure 9 (Munir et al., 2020). The samples display a type IV isotherm, creating a hysteresis loop at relative pressure P/P_0 between 0.1 and 0.30, implying the presence of microporous and mesoporous nanoparticles. High photocatalysis and efficient particle movement between reactant and product are possible with such designed porous structures. The sol-gel approach produced a V_2O_5 nanoparticle with a specific surface area of 89.211 M^2/gm, a pore diameter of 8.9675 nm, and a pore volume of 0.002 cc/gm.

Table 2: N_2 adsorption-desorption curve for surface area measurement of V_2O_5NPs

Parameters	value
Surface area (M^2/gm)	89.211
Slope	498.552
Intercept	8.057
Volume	0.002

4.6 Photocatalytic MB dye degradation of V_2O_5 photocatalyst

The photocatalytic activity of the V_2O_5 was examined in the presence of visible light after the contact time and catalyst dosage were optimized using methylene blue. As shown in Table 2, the MB dye removal effectiveness ranges from 69.59 to 97.54%. When the catalyst dosage was 20 mg/100 mL, the contact time was 60 min, and the initial MB concentration was 5 mg/L, the highest removal efficiency of 97.54% was achieved. The adsorption capacity was 4.9385 mg/g when the catalyst's dose was 20 mg/100 mL, the contact period was 60 min, and the MB concentration was 5 mg/L. Furthermore, 97.54% of the MB was removed using a catalyst dosage of 20 mg/100 mL; when the starting MB concentration was altered from the lower concentration to the higher one, the removal effectiveness was 76% while maintaining the same other parameters. Conversely, when the other two parameters are maintained at their optimal levels, increasing the catalyst dosage from 20 to 40 mg/100 mL produced a removal efficiency of 84.70%. This results in a reduction of 12.84% in removal efficiency. More significantly, it implies that the catalyst dosage has a greater impact than the initial MB concentration. Lastly, the removal performance of MB decreases with increasing catalyst dosage and contact time. But removal efficiency rises when the initial MB dye concentration decreases (Fito et al., 2023)(Babar et al., 2020).

Table 3: Photocatalytic performance of V_2O_5 photocatalyst for MB removal

	Factor 1	Factor 2	Factor 3	Response 1
Run	A: Initial concentration (ppm)	B: Catalyst dosage (mg)	C: Contact time (min)	Degradation efficiency (%)
1	5	20	20	93.01
2	5	20	40	94.78
3	5	20	60	97.54
4	5	20	80	93.15
5	10	20	20	88.98
6	10	20	40	90.15
7	10	20	60	93.35
8	10	20	80	85.25
9	15	20	20	73.86

10	15	20	40	75.1
11	15	20	60	81.88
12	15	20	80	80.15
13	5	30	20	78.04
14	5	30	40	85.66
15	5	30	60	92.68
16	5	30	80	87.56
17	10	30	20	77.85
18	10	30	40	82.08
19	10	30	60	88.62
20	10	30	80	80.25
21	15	30	20	70.84
22	15	30	40	75.04
23	15	30	60	81.88
24	15	30	80	78.1
25	5	40	20	73.62
26	5	40	40	80.74
27	5	40	60	84.7
28	5	40	80	81.98
29	10	40	20	72.77
30	10	40	40	77.025
31	10	40	60	84.09
32	10	40	80	82.17
33	15	40	20	69.59
34	15	40	40	74.92
35	15	40	60	76
36	15	40	80	72.35

4.6.1 Effect of contact time on MB dye degradation of V_2O_5 photocatalyst

The impact of contact time on the V_2O_5 degradation of MB dye is shown in Fig. 9. While maintaining a constant catalyst amount (20 mg) and dye concentration (5 ppm), the experiments were carried out under visible light at various contact time intervals (0 min to 80 min at a step size of 20 min). After reaching its maximum, the proportion of dye degradation remained nearly constant as time went on. This is because longer contact times between dye molecules and catalysts accelerate the breakdown process. Initially, there will be more active sites on the catalyst for the dye molecules to react with, but as more and more dye molecules adsorb onto the catalyst surface, the catalyst surface will eventually become saturated. Therefore, the longer period does not affect dye degradation (Chandrika et al., 2022).

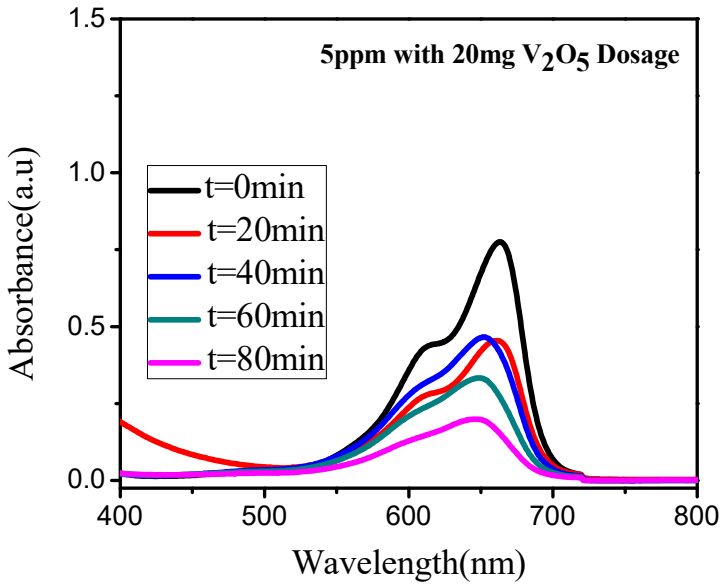

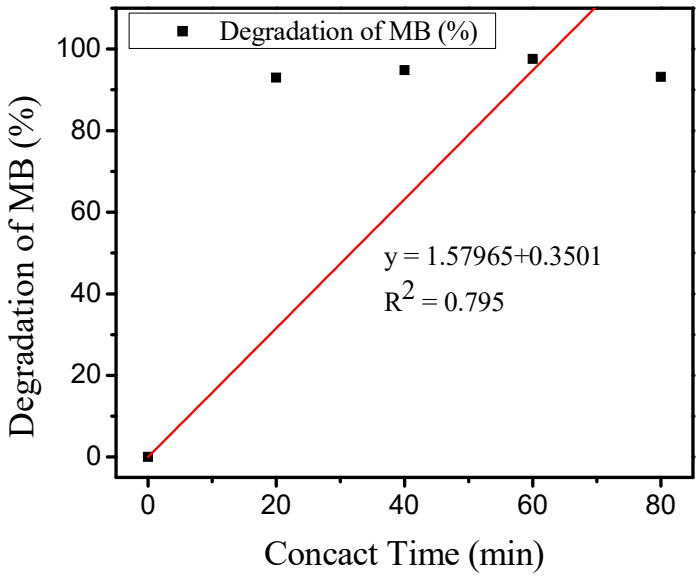

Figure 9: Effect of contact time on MB dye degradation of V_2O_5 photocatalyst

4.6.2 Effect of catalyst dosage

Loading of the photocatalyst is an important parameter that strongly affects photocatalytic performance. Raising the dosage of the catalyst tends to increase the efficiency of pollutant degradation, since larger active site availability on the photocatalyst- yst's surface favors the formation of reactive radicals. Exceeding an optimum level, though, may negatively impact performance. Higher dosages give rise to catalyst clumping, so fewer active sites become available for radical formation at the surface of the photocatalyst. Moreover, excess use of photocatalyst escalates turbidity, scattering, and absorbing incoming irradiation, so less penetrates the reaction volume. Such a shielding effect diminishes photon absorption needed for electron–hole (ecb^-/hvb^+) pair formation, thus ultimately predisposing towards recombination processes and reducing photocatalytic performance. As illustrated through Fig. 10 (a, b, and c), MB dye (initial concentration 5 mg/L) degradation was reduced at higher dosages of catalyst, increasing over and above the optimum dosage level. Photocatalytic efficiencies of 97.54%, 92.68%, and 84.70% corresponded to catalyst dosings of 20 mg, 30 mg, and 40 mg, respectively (Chandrika et al., 2022); (Fito et al., 2023).

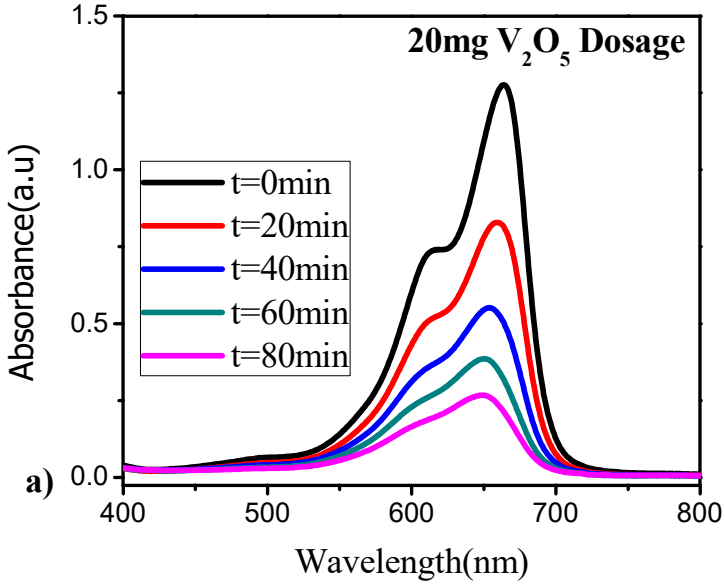
20mg V2O5 Dosage
t=0min
t=20min
t=40min
t=60min
t=80min
Absorbance(a.u)
Wavelength(nm)
a)
1.5
1.0
0.5
0.0
400
500
600
700
800

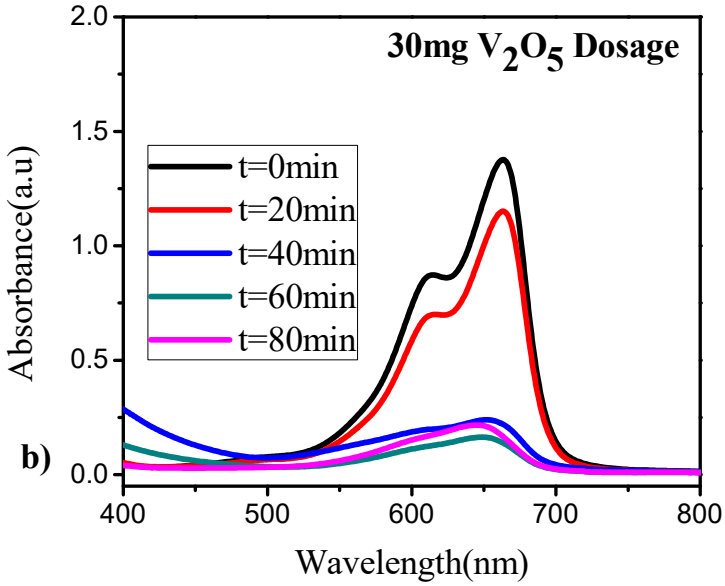
30mg V2O5 Dosage
t=0min
t=20min
t=40min
t=60min
t=80min
Absorbance(a.u)
Wavelength(nm)
b)
2.0
1.5
1.0
0.5
0.0
400
500
600
700
800

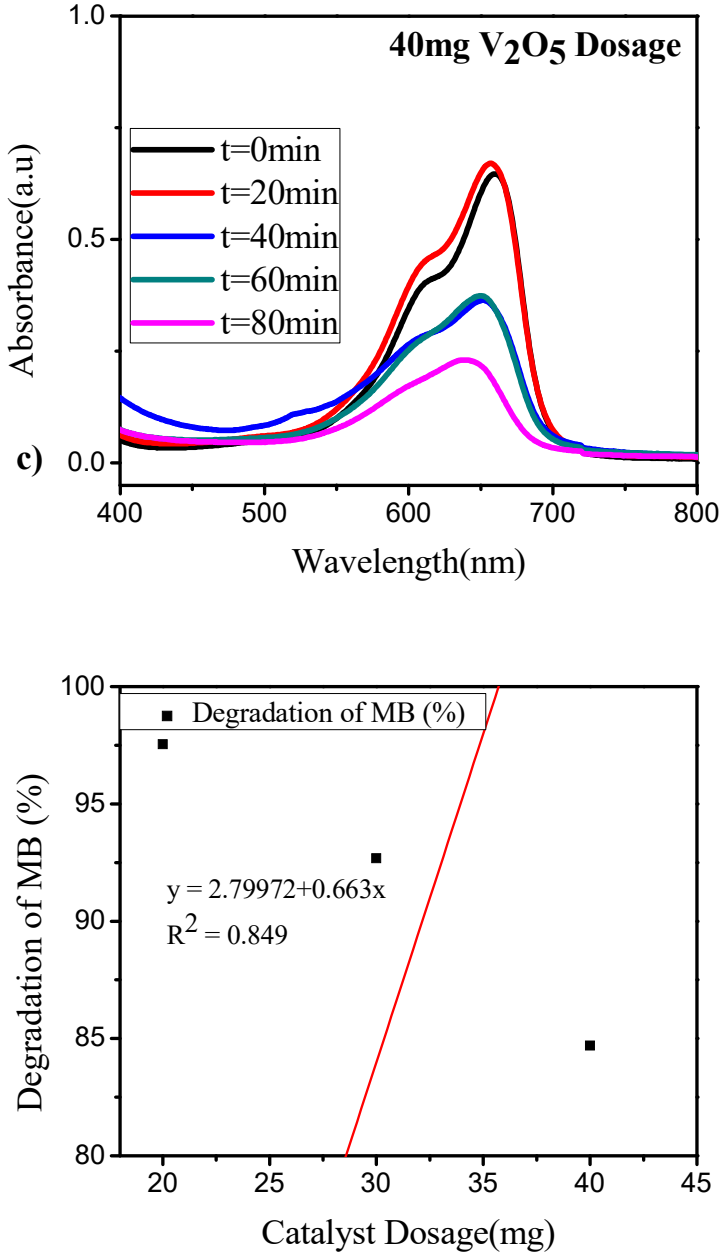

Figure 10: Effect of catalyst dosage

4.6.3 Effect of MB dye concentration

Figure 11 (a, b, and c) shows how different dye concentrations alter the percentage of degradation. The studies were carried out under visible light, with starting dye concentrations ranging from 5 ppm to 15 ppm in 5 ppm increments, and a catalyst dosage of 20 mg. Clearly, the degrading efficiency dropped as the MB concentration increased. Higher concentrations

prevent visible light from reaching the catalyst surface, decreasing the production of ·OH radicals. According to the pseudo-first-order kinetic model (see Figure 11d), the rate constant decreased from 0.05 min^{-1} at 5 mg/L to 0.03 min^{-1} at 15 mg/L as the reaction rates decreased with increasing MB concentration. Furthermore, because of the increased demand, higher MB concentrations could lead to insufficient ·OH radicals. An additional issue is that the numerous MB dye molecules absorb some photons, which lowers the number of photons available for the catalytic surface (Munir et al., 2020; Fito et al., 2023).

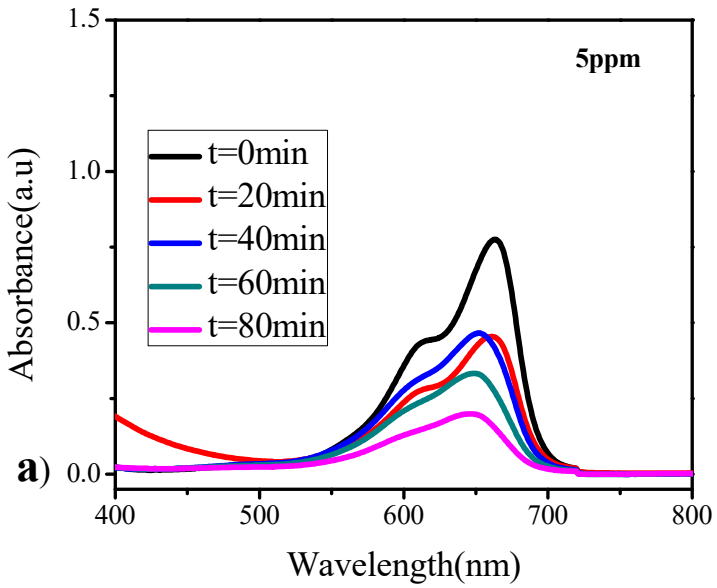

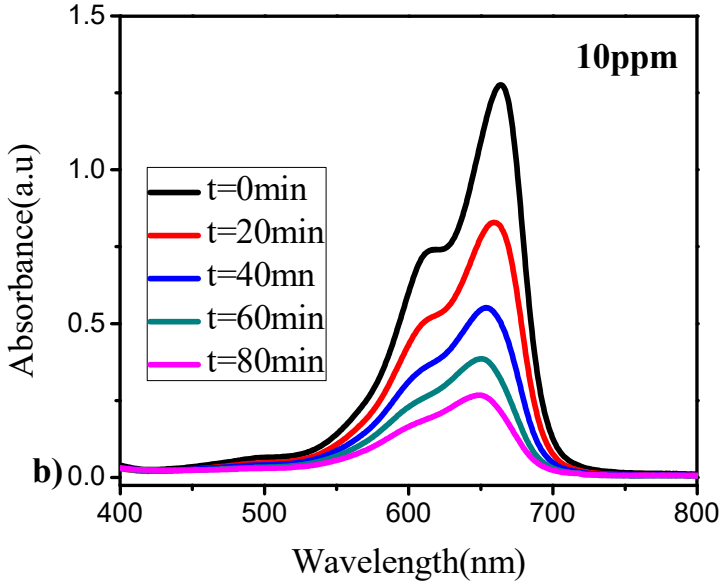
10ppm
t=0min
t=20min
t=40mn
t=60min
t=80min
Absorbance(a.u)
Wavelength(nm)
b)
1.5
1.0
0.5
0.0
400
500
600
700
800

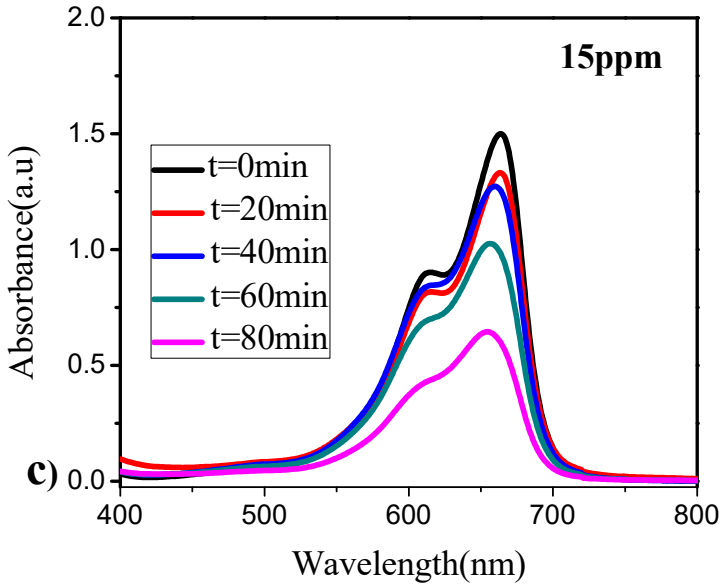
15ppm
t=0min
t=20min
t=40min
t=60min
t=80min
Absorbance(a.u)
Wavelength(nm)
c)
2.0
1.5
1.0
0.5
0.0
400
500
600
700
800

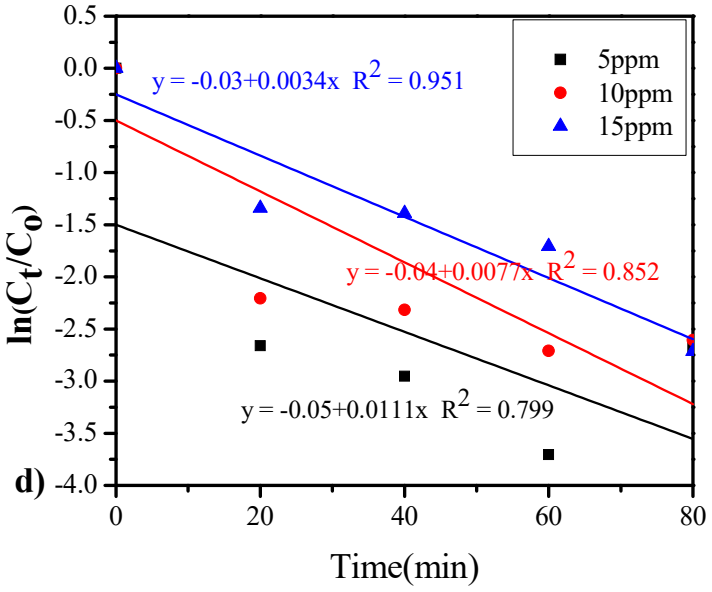

Figure 11: Effect of MB dye concentration at different initial concentrations

4.7 Interaction effects on the MB removal efficiencies

4.7.1 Initial MB concentration and catalyst dosage.

The effectiveness of eliminating contaminants from wastewater or an aqueous solution depends on the interplay of two or more variables in addition to individual parameters. The most appropriate model for forecasting removal efficiency, according to statistical analysis, is the interactive regression model. It was determined that all six of the interactions between the four independent variables were significant. As shown in Fig. 12, the interaction between the initial MB concentration and the catalyst dosage positively affects the overall removal performance of MB. Increasing the adsorbent alone enhances removal efficiency, while a higher MB concentration reduces it. Therefore, the catalyst dosage has a more significant effect than the initial MB concentration. Furthermore, the 3D graphical depiction demonstrates that the interaction between the catalyst dosage and initial MB concentration results in the maximum removal effectiveness of 97.54%. Conversely, the lowest projected removal efficiency is 69.59% (Fito et al., 2023; Saad et al., 2021).

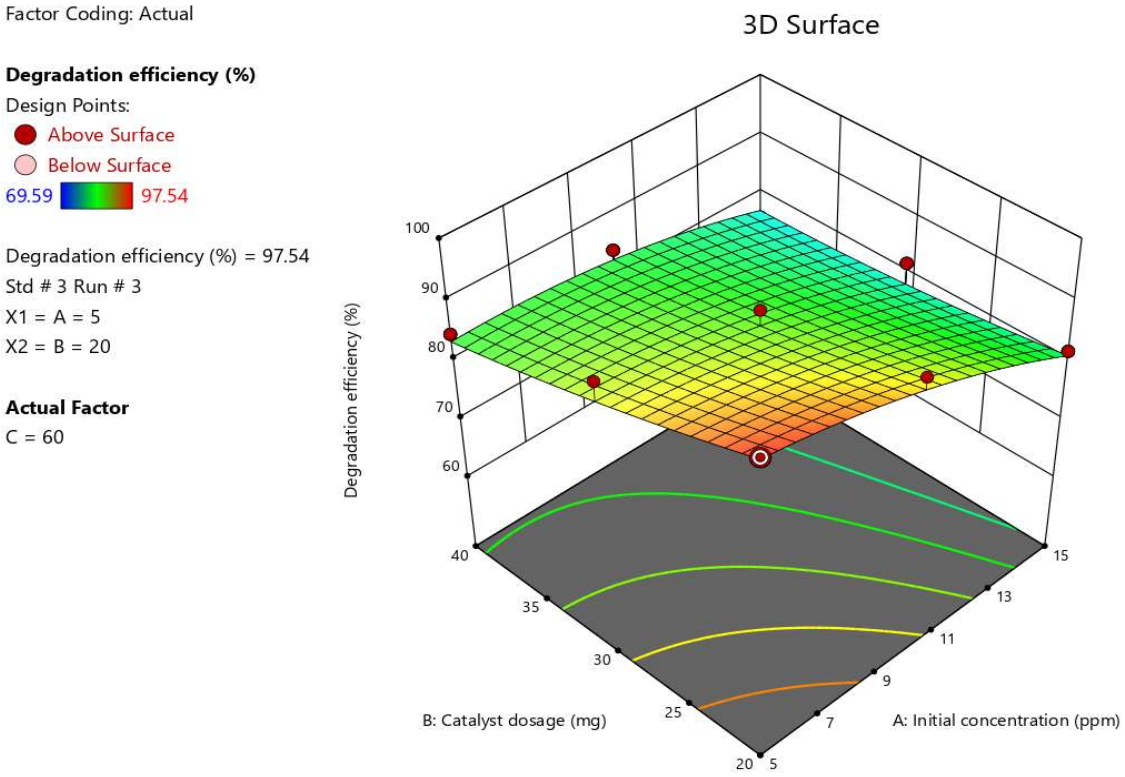

Figure 12: Interaction effects of initial MB concentration and catalyst dosage

4.7.2 Adsorbent dosage and contact time

To assess the combined impact of the amount of adsorbent and contact duration on the removal of methylene blue (MB), RSM (response surface method) was used. The experiments were conducted at a fixed median initial MB concentration while varying the adsorbent dosage and contact time, as illustrated in Fig. 13. The 3D interaction plot revealed a synergistic effect: increasing either the adsorbent dosage or the contact time individually resulted in higher MB removal efficiency. The predicted removal efficiency ranged from 69.59% to 97.54%, with the maximum of 97.54% achieved at an adsorbent dosage of 20 mg/100 mL and a contact time of 60 minutes. The close agreement between the predicted and experimental values indicates that the model accurately represents the adsorption process. (Babar et al., 2020; Fito et al., 2023; Kruefu et al., 2017).

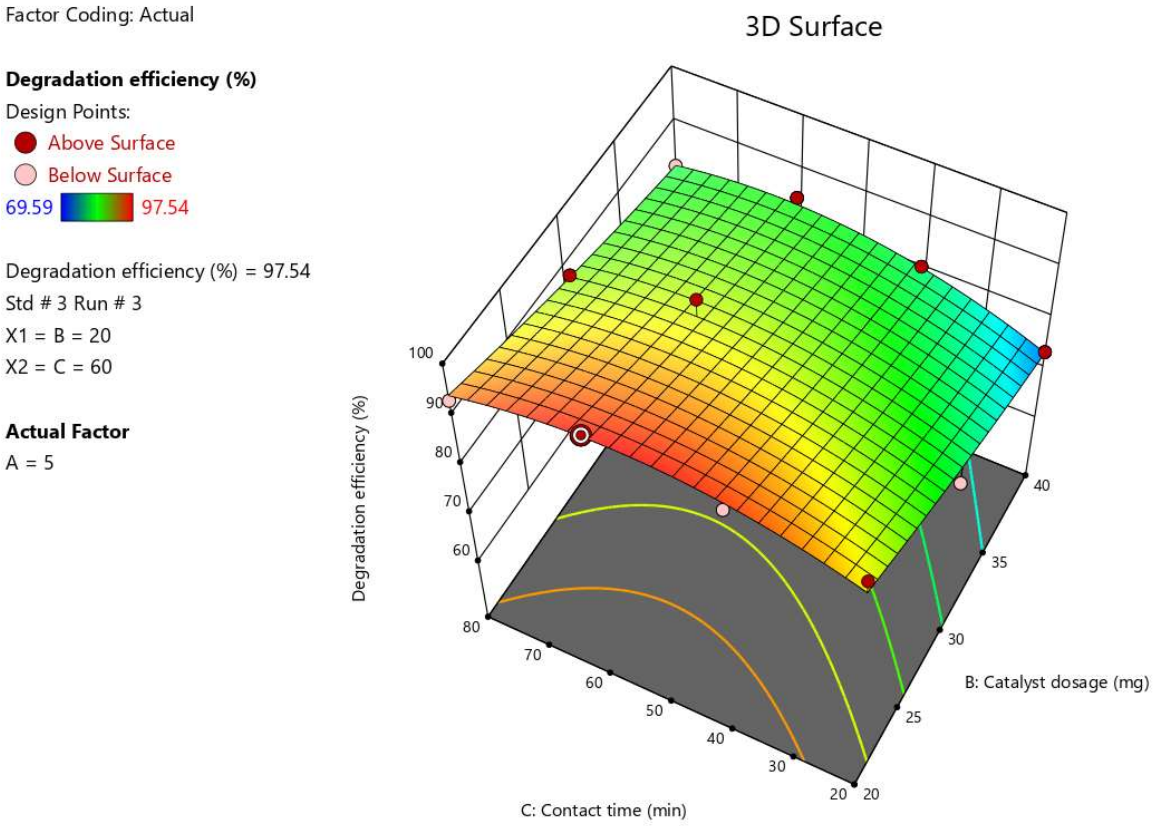

Figure 13: Interaction effects of catalyst dosage and contact time

4.7.3 Contact Time and Initial Dye Concentration

Figure 14 illustrates how the duration of irradiation and the initial concentration of dye affect the percentage of dye degradation. When the initial dye concentration is 5 ppm, the percentage of dye degradation rises as the irradiation time increases. Extending the irradiation time to 60 minutes results in greater dye degradation because more photons are absorbed by the catalyst surface, which boosts the reactive oxygen species responsible for photodegradation, thereby enhancing dye degradation (Babar et al., 2020; Fito et al., 2023; Kruefu et al., 2017).

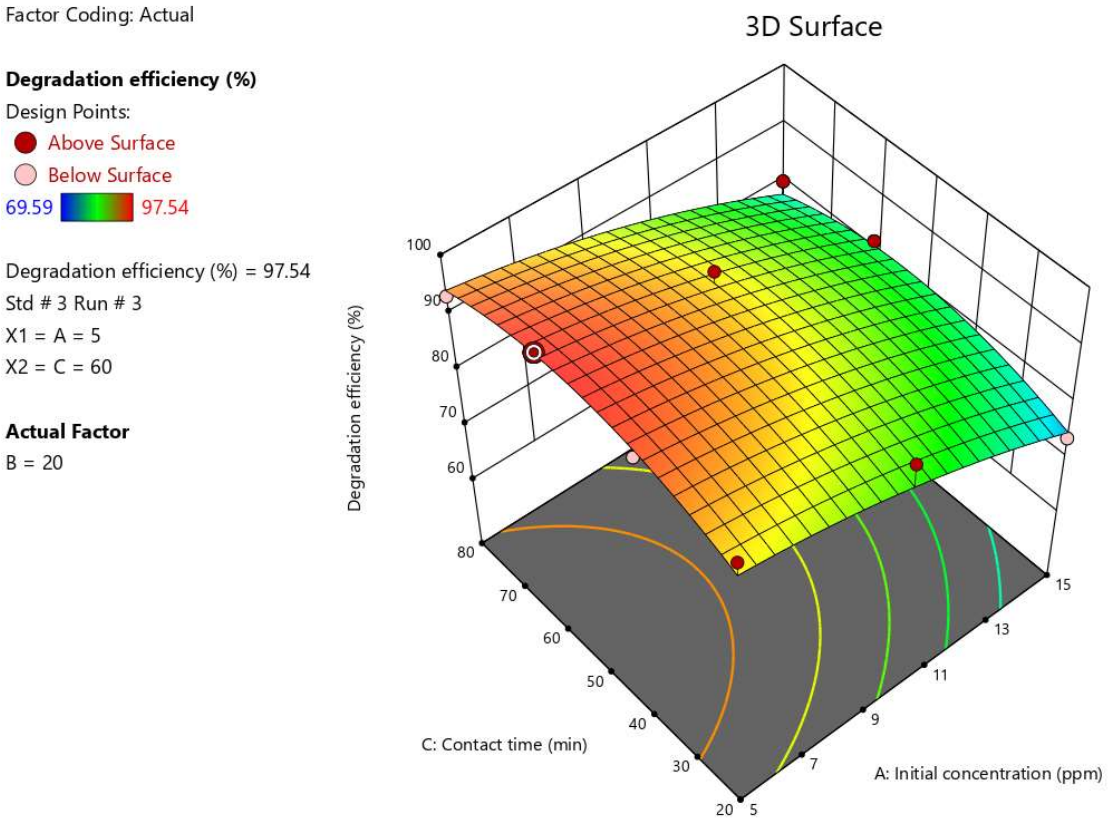

Figure 14: Interaction effects of contact time and initial dye concentration

4.8 Design of Experiments and Response Surface Method

The association among the factors and the variables that responded was ascertained by the statistical technique of multiple regression. Several models, including two-way, square, and linear interaction models, were fitted to the user-defined response values. The model is significant, according to the ANOVA findings (Table 4), with low p-values < 0.05 and an R^2 value of 0.8875.As demonstrated in Table 4, the experimental and predicted response values are also linked, confirming the statistical validity of the experimental data.

Table 4 : Analysis of variance (ANOVA) results of the model

Source	Sum of Squares	df	Mean Square	F-value	p-value	
Model	1809.89	9	201.10	31.69	< 0.0001	significant

A-Initial concentration	745.38	1	745.38	117.46	< 0.0001	
B-Catalyst dosage	572.77	1	572.77	90.26	< 0.0001	
C-Contact time	165.21	1	165.21	26.03	< 0.0001	
AB	96.58	1	96.58	15.22	0.0006	
AC	0.1449	1	0.1449	0.0228	0.8811	
BC	23.25	1	23.25	3.66	0.0667	
A^2	37.56	1	37.56	5.92	0.0222	
B^2	5.53	1	5.53	0.8715	0.3591	
C^2	163.48	1	163.48	25.76	< 0.0001	
Residual	164.99	26	6.35			
Cor Total	1974.89	35				

5 CONCLUSION AND RECOMMENDATION

5.1 Conclusion

V_2O_5 nanoparticles were synthesized *by Laggera tomentosa* plant leaf extracts via the sol-gel method. The XRD analysis presented the orthorhombic pure V_2O_5 nanoparticle. The UV-Vis DRS analysis revealed a V_2O_5 band gap energy of 2.94 eV. The mesoporous particles have a smooth surface, and all of the particles shown in the SEM micrographs are nano-sized. This adsorbent exhibited good adsorption properties, such as a large surface area, a favorable surface shape, and multifunctionality. To improve photocatalytic efficiency, the response surface methodology was integrated with the user-defined model approach. The range of MB removal efficiency was 69.59% to 97.54%. Under verified settings of 60 minutes of contact time, 5 mg/L of initial MB concentration, and 20 mg/100 mL of catalyst dosage, the highest removal efficacy of 97.54% was attained. Nonetheless, further research should be done before pilot-scale testing and the use of industrial wastewater treatment, including column analysis, adsorbent combination with magnetic material, catalyst development optimization, and thermodynamics investigation.

5.2 Recommendation

For future research, there are a few recommendations on the characterization of V_2O_5 nanoparticles that will provide full information. Based on the present findings, V_2O_5 nanoparticles were synthesized by *Laggera tomentosa* plant leaf extracts. The surface of the V_2O_5 nanoparticle catalyst highly adsorbs the pollutants. The elemental distribution and chemical content of manufactured materials should be determined using energy dispersive X-ray (EDX) and X-ray photoelectron spectroscopy (XPS). To explore the morphology of nanoparticles in greater depth, the samples should be described using TEM. The influence of pH on MB dye degradation in V_2O_5 photocatalysis should be investigated, as well as the effect of solution temperature. Scavengers should also be used during photoreaction to determine which reactive species are primarily engaged in the MB's photodegradation.

REFERENCE

Abuzeid, H. M., Moustafa, A. M., & Hashem, A. M. (2021). Global Journal of Chemical Sciences One-Step Green Synthesis of V_2O_5 and VO_2 Using Extract of Orange Peel : Effect of Calcination Atmosphere. 1(1), 1–7.

Agarwal, H., Venkat Kumar, S., & Rajeshkumar, S. (2017). A review on green synthesis of zinc oxide nanoparticles – An eco-friendly approach. Resource-Efficient Technologies, 3(4), 406–413. https://doi.org/10.1016/j.reffit.2017.03.002

Ahmad, N., & Sharma, S. (2012). Green Synthesis of Silver Nanoparticles Using Extracts of; Green and Sustainable Chemistry, 02(04), 141–147. https://doi.org/10.4236/gsc.2012.24020

Aliyu, A. O., Garba, S., & Bognet, O. (2017). Green Synthesis, Characterization and Antimicrobial Activity of Vanadium Nanoparticles using Leaf Extract of Moringa oleifera. International Journal of Chemical Sciences Research, 16(1), 231.

Babar, B. M., Mohite, A. A., Patil, V. L., Pawar, U. T., Kadam, L. D., Kadam, P. M., & Patil, P. S. (2020). Materials Today : Proceedings Sol-gel prepared vanadium oxide for photocatalytic degradation of Methylene Blue dye. Materials Today: Proceedings, xxxx, 1–5. https://doi.org/10.1016/j.matpr.2020.04.205

Babar, B. M., Pisal, K. B., Sutar, S. H., Kadam, L. D., Pathan, H. M., Pawar, U. T., Kadam, P. M., & Patil, P. S. (2022). Hydrothermally Prepared Vanadium Oxide Nanostructures for Photocatalytic Application. ES Energy & Environment, 82–91. https://doi.org/10.30919/esee8c639

Basfer, N. M., Mansour, S. F., & Ahmed, M. K. (2021). Physicochemical properties of hydroxyapatite modified with vanadium ions for degradation of methylene blue. Journal of Molecular Structure, 1240, 130562. https://doi.org/10.1016/j.molstruc.2021.130562

Baudot, C., Tan, C. M., & Kong, J. C. (2010). FTIR spectroscopy as a tool for nano-material characterization. Infrared Physics and Technology, 53(6), 434–438. https://doi.org/10.1016/j.infrared.2010.09.002

Benhadria, N., Hachemaoui, M., Zaoui, F., Mokhtar, A., Boukreris, S., Attar, T., Belarbi, L., & Boukoussa, B. (2022). Catalytic Reduction of Methylene Blue Dye by Copper Oxide Nanoparticles. Journal of Cluster Science, 33(1), 249–260. https://doi.org/10.1007/s10876-020-01950-0

Buckner, C. A., Lafrenie, R. M., Dénommée, J. A., Caswell, J. M., Want, D. A., Gan, G. G., Leong, Y. C., Bee, P. C., Chin, E., Teh, A. K. H., Picco, S., Villegas, L., Tonelli, F., Merlo, M., Rigau, J., Diaz, D., Masuelli, M., Korrapati, S., Kurra, P., … Mathijssen, R. H. J. (2016a). We are IntechOpen , the world ' s leading publisher of Open Access books Built by scientists , for scientists TOP 1 %. In Intech (Vol. 11, Issue tourism, p. 13). https://www.intechopen.com/books/advanced-biometric-technologies/liveness-detection-in-biometrics

Chandrika, K. C., Prabhu, T. N., Kiran, R. R. S., & Krishna, R. H. (2022). Applications of artificial neural network and Box-Behnken Design for modelling malachite green dye degradation from textile effluents using TiO_2 photocatalyst. 27(1), 0–3.

Corr, S. A. (2012). Metal oxide nanoparticles. 180–207. https://doi.org/10.1039/9781849734844-00180

Demissie, M. G., Sabir, F. K., Edossa, G. D., & Gonfa, B. A. (2020). Synthesis of Zinc Oxide Nanoparticles Using Leaf Extract of Lippia adoensis (Koseret) and Evaluation of Its Antibacterial Activity. 2020.

Din, M. I., Arshad, F., Hussain, Z., & Mukhtar, M. (2017). Green Adeptness in the Synthesis and Stabilization of Copper Nanoparticles : Catalytic , Antibacterial , Cytotoxicity , and Antioxidant Activities. https://doi.org/10.1186/s11671-017-2399-8

Drummer, S., Madzimbamuto, T., & Chowdhury, M. (2021). Green synthesis of transition-metal nanoparticles and their oxides: A review. Materials, 14(11). https://doi.org/10.3390/ma14112700

Farahmandjou, M. (2017). Chemical Synthesis of Vanadium Oxide (V_2O_5) Nanoparticles Prepared by Sodium Metavanadate. Journal of Nanomedicine Research, 5(1), 2–5. https://doi.org/10.15406/jnmr.2017.05.00103

Fito, J., Abewaa, M., Mengistu, A., Angassa, K., Ambaye, A. D., Moyo, W., & Nkambule, T. (2023). Adsorption of methylene blue from textile industrial wastewater using activated carbon developed from Rumex abyssinicus plant. Scientific Reports, 1–17. https://doi.org/10.1038/s41598-023-32341-w

Getahun, T., Sharma, V., Kumar, D., & Gupta, N. (2020). Chemical composition, and antibacterial and antioxidant activities of essential oils from Laggera tomentosa Sch. Bip. ex Oliv. et Hiern (Asteraceae). Turkish Journal of Chemistry, 44(6), 1539–1548. https://doi.org/10.3906/kim-2004-50

Hassan, Z., & Rasheed, R. (2021). Preparation of V_2O_5 and SnO_2 Nanoparticles and Their Application as Pollutant Removal. Journal of Applied Sciences and Nanotechnology, 1(4), 69–80. https://doi.org/10.53293/jasn.2021.3869.1049

Jemal, K., Sandeep, B. V., & Pola, S. (2017). Synthesis, Characterization, and Evaluation of the Antibacterial Activity of Allophylus serratus Leaf and Leaf Derived Callus Extracts Mediated Silver Nanoparticles. Journal of Nanomaterials, 2017. https://doi.org/10.1155/2017/4213275

Kammakakam, I. (2021). As featured in : Materials Advances. https://doi.org/10.1039/d0ma00807a

Khan, I., Saeed, K., & Khan, I. (2017). Arabian Journal of Chemistry, May. https://doi.org/10.1016/j.arabjc.2017.05.011

Kruefu, V., Sintuya, H., Pookmanee, P., & Phanichphant, S. (2017). Visible Light Photocatalytic Degradation of Methylene Blue Using V_2O_5 Nanoparticles. V, 62–67.

Li, Y., Kuang, J. L., Lu, Y., & Cao, W. Bin. (2017). Facile synthesis, characterization of flower-like vanadium pentoxide powders and their photocatalytic behavior. Acta Metallurgica Sinica (English Letters), 30(10), 1017–1026. https://doi.org/10.1007/s40195-017-0611-6

Liu, Y., Chen, Q., Du, X., Liu, X., & Li, P. (2019). Effects of substrate on the structure and properties of V_2O_5 thin films prepared by the sol-gel method. AIP Advances, 9(4). https://doi.org/10.1063/1.5095718

Mohamed, A., & Shafey, E. (2020). Shafey2020.Pdf. 304–339.

Munir, M., Akthar, N., Javed, Y., & Bashir, S. (2020). Preparation and characterization of Vanadium pentoxide (V_2O_5) for photocatalytic degradation of monoazo and diazo dyes. Surfaces and Interfaces, 19(February), 100502. https://doi.org/10.1016/j.surfin.2020.100502

Nguyen, N. H. A., Padil, V. V. T., Slaveykova, V. I., Černík, M., & Ševců, A. (2018). Green Synthesis of Metal and Metal Oxide Nanoparticles and Their Effect on the Unicellular Alga Chlamydomonas reinhardtii. Nanoscale Research Letters, 13. https://doi.org/10.1186/s11671-018-2575-5

Rafique, M., Hamza, M., Tahir, M. B., Muhammad, S., & Al-Sehemi, A. G. (2020). Facile hydrothermal synthesis of highly efficient and visible light-driven Ni-doped V_2O5 photocatalyst for degradation of Rhodamine B dye. Journal of Materials Science: Materials in Electronics, 31(15), 12913–12925. https://doi.org/10.1007/s10854-020-03844-3

Rafique, M., Sadaf, I., Rafique, M. S., & Tahir, M. B. (2016). A review on green synthesis of silver nanoparticles and their applications. Artificial Cells, Nanomedicine, and Biotechnology, 0(0), 000. https://doi.org/10.1080/21691401.2016.1241792

Saad, R. A., Younes, G., & Rami, M. H. E. (2021). Vanadium-Substituted Polyoxomolybdates for Methylene Blue Adsorption from Aqueous Solutions. Journal of Cluster Science, 4. https://doi.org/10.1007/s10876-021-02130-4

Sajid, M. M., Shad, N. A., Javed, Y., Khan, S. B., Zhang, Z., Amin, N., & Zhai, H. (2020). Preparation and characterization of Vanadium pentoxide (V_2O_5) for photocatalytic degradation of monoazo and diazo dyes. Surfaces and Interfaces, 19, 100502. https://doi.org/10.1016/j.surfin.2020.100502

Shanker, U., Jassal, V., & Rani, M. (2016). Catalytic removal of organic colorants from water using some transition metal oxide nanoparticles synthesized under sunlight. RSC Advances, 6(97), 94989–94999. https://doi.org/10.1039/c6ra17555d

Singh, N. B. (2022). Green synthesis of nanomaterials. Handbook of Microbial

Nanotechnology, 225–254. https://doi.org/10.1016/B978-0-12-823426-6.00007-3

T.R. Kishan Chand, H.M. Kalpana 1,*, H. S. L. 2 1Department. (2022). Green synthesis of vanadium oxide nanoparticles for thin film based sensor application Green synthesis of vanadium oxide nanoparticles for thin film based sensor application. Mater. Sci. Eng. https://doi.org/10.1088/1757-899X/1225/1/012062

Talavera, N., Navarro, M., Boada-sucre, A. A., & Gonzalez, I. (2013). Green synthesis of nanosized vanadium pentoxide using Saccharomyces cerevisiae as biotemplate. Recent Res. Devel. Mat. Sci., 10(December 2014), 89–102.

Uddin, M. N., Rahman, S., Shumi, W., Hossain, K., & Ullah, A. K. M. A. (2020). Characterization , microbial and catalytic application of V_2O_5 nanoparticles prepared from Schiff base complexes as precursor. Journal of Chemical Sciences, 0123456789. https://doi.org/10.1007/s12039-020-01840-y

Vo, T. N., Kim, H., Hur, J., Choi, W., & Kim, I. T. (2018). Surfactant-assisted ammonium vanadium oxide as a superior cathode for calcium-ion batteries. Journal of Materials Chemistry A, 6(45), 22645–22654. https://doi.org/10.1039/c8ta07831a

Whitfield, P., & Mitchell, L. (2004). X-ray diffraction analysis of nanoparticles: Recent developments, potential problems and some solutions. International Journal of Nanoscience, 3(6), 757–763. https://doi.org/10.1142/S0219581X04002620

Ying, S., Guan, Z., Ofoegbu, P. C., Clubb, P., Rico, C., He, F., & Hong, J. (2022). Green synthesis of nanoparticles: Current developments and limitations. Environmental Technology and Innovation, 26, 102336. https://doi.org/10.1016/j.eti.2022.102336

Zhang, Y., Zhang, X., Zhang, L., Alarfaj, A. A., Hirad, A. H., & Alsabri, A. E. (2021). Green formulation, chemical characterization, and antioxidant, cytotoxicity, and anti-human cervical cancer effects of vanadium nanoparticles: A pre-clinical study. Arabian Journal of Chemistry, 14(6), 103147. https://doi.org/10.1016/j.arabjc.2021.103147

APPENDICES

Appendix 1: Table for full factorial experimental matrix for degradation of MB dye in percent and Adsorption capacity (qt)of the MB dye onto V_2O_5 nanoparticle

run	C_o (ppm)	Dosage (gm)	contact time (min)	C_t (ppm)	Removal (%)	q_t (mg/g)
1	5	0.02	20	0.3495	93.01	4.82525
2	5	0.02	40	0.261	94.78	4.8695
3	5	0.02	60	0.123	97.54	4.9385
4	5	0.02	80	0.3425	93.15	4.82875
5	10	0.02	20	1.102	88.98	9.449
6	10	0.02	40	0.985	90.15	9.5075
7	10	0.02	60	0.665	93.35	9.6675
8	10	0.02	80	0.7375	85.25	9.63125
9	15	0.02	20	3.921	73.86	13.0395
10	15	0.02	40	3.735	75.1	13.1325
11	15	0.02	60	2.718	81.88	13.641
12	15	0.02	80	0.9925	80.15	14.50375
13	5	0.03	20	1.098	78.04	4.634
14	5	0.03	40	0.717	85.66	4.761
15	5	0.03	60	0.366	92.68	4.878
16	5	0.03	80	0.622	87.56	4.792666667
17	10	0.03	20	2.215	77.85	9.261666667
18	10	0.03	40	1.792	82.08	9.402666667
19	10	0.03	60	1.138	88.62	9.620666667
20	10	0.03	80	0.9875	80.25	9.670833333
21	15	0.03	20	4.374	70.84	13.542
22	15	0.03	40	3.744	75.04	13.752
23	15	0.03	60	2.718	81.88	14.094
24	15	0.03	80	1.095	78.1	14.635

25	5	0.04	20	1.319	73.62	4.67025
26	5	0.04	40	0.9635	80.74	4.759125
27	5	0.04	60	0.765	84.7	4.80875
28	5	0.04	80	0.901	81.98	4.77475
29	10	0.04	20	2.723	72.77	9.31925
30	10	0.04	40	2.2975	77.025	9.425625
31	10	0.04	60	1.591	84.09	9.60225
32	10	0.04	80	0.8915	82.17	9.777125
33	15	0.04	20	4.5615	69.59	13.859625
34	15	0.04	40	3.762	74.92	14.0595
35	15	0.04	60	3.6	76	14.1
36	15	0.04	80	1.3825	72.35	14.654375

Appendix 2: Table of model report for full factorial experimental matrix for degradation of MB dye in percent onto V_2O_5 nanoparticle

Run Order	Actual Value	Predicted Value	Residual	Leverage	Internally Studentized Residuals	Externally Studentized Residuals	Cook's Distance	Influence on Fitted Value DFFITS	Standard Order
1	93.01	90.79	2.22	0.429	1.169	1.177	0.103	1.021	1
2	94.78	96.15	-1.37	0.251	-0.630	-0.622	0.013	-0.361	2
3	97.54	97.26	0.2822	0.251	0.129	0.127	0.001	0.074	3
4	93.15	94.10	-0.9510	0.429	-0.500	-0.492	0.019	-0.427	4

5	88.98	85.03	3.95	0.292	1.865	1.965	0.143	1.261	5
6	90.15	90.32	-0.1743	0.181	-0.076	-0.075	0.000	-0.035	6
7	93.35	91.36	1.99	0.181	0.873	0.869	0.017	0.408	7
8	85.25	88.13	-2.88	0.292	-1.360	-1.384	0.076	-0.888	8
9	73.86	74.93	-1.07	0.429	-0.565	-0.557	0.024	-0.483	9
10	75.10	80.16	-5.06	0.251	-2.323	-2.558	0.181	-1.483	10
11	81.88	81.13	0.7513	0.251	0.345	0.339	0.004	0.196	11
12	80.15	77.83	2.32	0.429	1.217	1.229	0.111	1.066	12
13	78.04	81.29	-3.25	0.292	-1.534	-1.577	0.097	-1.012	13
14	85.66	87.54	-1.88	0.181	-0.824	-0.819	0.015	-0.384	14
15	92.68	89.52	3.16	0.181	1.384	1.410	0.042	0.662	15
16	87.56	87.25	0.3119	0.292	0.147	0.144	0.001	0.093	16
17	77.85	77.99	-0.1394	0.217	-0.063	-0.061	0.000	-0.032	17
18	82.08	84.17	-2.09	0.172	-0.911	-0.908	0.017	-0.414	18
19	88.62	86.08	2.54	0.172	1.107	1.112	0.025	0.507	19

20	80.25	83.74	-3.49	0.217	-1.564	-1.612	0.068	-0.848	20
21	70.84	70.35	0.4859	0.292	0.229	0.225	0.002	0.144	21
22	75.04	76.46	-1.42	0.181	-0.624	-0.616	0.009	-0.289	22
23	81.88	78.31	3.57	0.181	1.566	1.613	0.054	0.757	23
24	78.10	75.89	2.21	0.292	1.041	1.042	0.045	0.669	24
25	73.62	73.46	0.1599	0.429	0.084	0.082	0.001	0.071	25
26	80.74	80.59	0.1519	0.251	0.070	0.068	0.000	0.040	26
27	84.70	83.45	1.25	0.251	0.572	0.564	0.011	0.327	27
28	81.98	82.06	-0.0781	0.429	-0.041	-0.040	0.000	-0.035	28
29	72.77	72.62	0.1550	0.292	0.073	0.072	0.000	0.046	29
30	77.03	79.67	-2.65	0.181	-1.161	-1.170	0.030	-0.549	30
31	84.09	82.47	1.62	0.181	0.710	0.704	0.011	0.330	31
32	82.17	81.00	1.17	0.292	0.550	0.542	0.012	0.348	32
33	69.59	67.44	2.15	0.429	1.131	1.138	0.096	0.987	33
34	74.92	74.43	0.4945	0.251	0.227	0.223	0.002	0.129	34

35	76.00	77.15	-1.15	0.251	-0.529	-0.521	0.009	-0.302	35
36	72.35	75.62	-3.27	0.429	-1.717	-1.788	0.222	-1.550	36